STScI | SPACE TELESCOPE SCIENCE INSTITUTE

JWST TECHNICAL REPORT

Title: NIRISS Commissioning Results: Imaging Photometric Calibration	Doc #: JWST-STScI-008269, SM-12 Date: 31 October 2022 Rev:
Authors: Kevin Volk and the NIRISS Team Phone: 410-338-4409	Release Date: 14 November 2022

1.0 Abstract

A number of observations of photometric standard stars were taken in the commissioning of NIRISS, most in program NIS-020/APT 01094. This report describes the reduction and analysis of these observations. A separate report by Goudfrooij et al. (2022) describes an analysis of the same observations using independent measuring methods, which were used as a check on the measurements presented here. The Goudfrooij et al. report concentrates on comparisons with pre-launch predictions, while the current report focuses on the determination of the conversion between count rate and surface brightness in physical units.

2.0 Introduction

Commissioning program NIS-020, APT program 1094, was devoted to the photometric calibration measurements for NIRISS imaging. The program consists of observations of photometric standards in the different NIRISS imaging configurations. The goal of this program is to produce the conversion factors from the observed signal in ADU/s to units of MJy/steradian that are required by the photometric calibration step in the JWST data reduction pipeline. For each imaging filter the conversion factor is assumed to be independent of the source and of position in the field of view.

Due to the sensitivity of NIRISS most of the photometric standard stars listed in the CALSPEC pages (https://www.stsci.edu/hst/instrumentation/reference-data-for-calibration-and-tools/astronomical-catalogs/calspec; see Bohlin, Gordon and Tremblay (2014)) are too bright to observe in all the imaging filters using full frame read-out without saturation issues. As a result, most of the observations need to be taken in smaller calibration sub-arrays that are not available for science observations. The commissioning observations in program 01094 reported here use two of the standard stars: LDS 749B (type DBQ4) and GSPC P330-E (type G2V) were observed.

Observations for NIS-020 were taken on two dates (25 May, 2022, and 6 June, 2022). Two epochs were used to make an initial determination of the stability of NIRISS for imaging observations.

In addition to the measurements in program NIS-020, a group of "early" photometric observations were taken in late March. These observations were not originally in the commissioning plan but were added to make an initial assessment of the instrument sensitivities. For NIRISS the observations were take using photometric standard stars

GSPC P177-D (type G0V), WD 1057+719 (type DA1.2) in a sub-set of the imaging filters. These observations were taken on 26 March, 2022 under program 01080.

Finally, there are a few acquisition images of the photometric standard BD+60°1753 (type A0mA1V) for the SOSS mode photometric calibration in program NIS-017/01092 which are also measured for completeness. All these measurements are in the F480M filter used for SOSS and AMI mode acquisitions.

3.0 Measured Quantities

The on-sky observations for program NIS-020 are simple. For each star and each filter configuration a series of exposures is taken with a two-point dither pattern to move the star with respect to the bad pixels in the detector. The data undergoes the standard level 1 reduction to produce a rate image with each pixel recording the mean rate for the exposures in units of ADU/s. The rate images are then run through the world coordinate system and flat field steps of the pipeline. The subsequent normal reduction steps are skipped. The flat-fielded rate images are used in the measurements. No attempt was made to combine the images from the two dither steps because we wish to avoid any type of image resampling.

As the desired units are surface brightness units, the image mean pixel area projected on the sky is also required for these calculations. The mean pixel area values are obtained from the PIXAR_A2 header keyword in the distortion reference appropriate to the imaging filter. These pixel areas were determined in program NIS-011a/APT 01086. It is assumed that the flat fielding step will correct for the effects of any variation of the projected pixel area on the sky over the field of view on the signal rate.

3.1 Mean Flux Density

The units for the photometricly calibrated images are given as surface brightness values in units MJy/steradian. However, the "flux density" used here is not the actual flux density at some given wavelength within the filter bandpass, but rather is an average of the flux density values weighted response and the object spectrum. If we define $\phi(\nu)$ as the number of electrons out at the detector per photon in at the primary mirror of JWST, the value of concern is the "photon-weighted mean flux density" given by

$$\overline{F_\nu} = \frac{\int F_\nu \phi(\nu) d\nu/\nu}{\int \phi(\nu) d\nu/\nu} \tag{1}$$

which is proportional to the integrated photon count rate for the source. This flux density value is **not** the object flux density at some specific wavelength that can be identified, although it must be equal to the actual object flux density at 1 or more wavelengths within the filter bandpass. The analogous wavelength mean flux density is given by

$$\overline{F_\lambda} = \frac{\int F_\lambda \lambda \phi(\lambda) d\lambda}{\int \lambda \phi(\lambda) d\lambda} \tag{2}$$

The wavelength at which $\overline{F_\lambda}$ and $\overline{F_\nu}$ are related by the usual equation $\lambda\overline{F_\lambda} = \nu\overline{F_\nu}$ is the pivot wavelength. This wavelength is generally quoted with the mean flux density, but it is important to remember that this is only for convenience in transforming from mean

frequency flux density to mean wavelength flux density. The formula for the pivot wavelength is

$$\lambda_p = \sqrt{\frac{\int_0^\infty \lambda\phi(\lambda)d\lambda}{\int_0^\infty \frac{1}{\lambda}\phi(\lambda)d\lambda}} \quad (3)$$

The mean flux density values $\overline{F_\lambda}$ and $\overline{F_\nu}$ are both strictly proportional to the count rate in ADU/s measured on the detector (implicitly assuming that the linearity correction is properly applied to the data). The corresponding surface brightness quantities also strictly proportional to the count rate if the flat fielding takes out the pixel area variations properly. This is assumed to be the case for NIRISS imaging, because of the way the flat field reference images are corrected to the on-sky illumination in program NIS-011a.

The NIRISS total photon conversion efficiency functions $\phi(\nu)$ and $\phi(\lambda)$ used in the calculations of the mean flux density values were the pre-flight values from ground testing. Post-commissioning analysis of the NIRISS response identified some discrepancies between the assumed throughput functions and the actual NIRISS on-sky performance. These changes in our estimate of $\phi(\lambda)$ produce small changes in the $\overline{F_\lambda}$ and $\overline{F_\nu}$ values. This then requires a small correction to the photometric calibration values. The post-commissioning changes to the photometric calibration as a result of the revisions in the estimated NIRISS response are not discussed further in this report. Those changes are of generally small magnitude (typically of the order of 0.1%) and so are somewhat smaller than the uncertainties in the initial photometric calibration values. Those revisions were not included in the photometric reference file submitted to CRDS for the pipeline at the end of commissioning.

3.2 Pixel Area Values

The mean pixel areas determined from program NIS-011a/APT 10186 are listed in Table 1 below as were delivered to the pixel area map reference file for the JWST pipeline. The number of decimal places listed is rather more than is actually required.

Table 1: List of the mean pixel areas of the imaging filters as derived in commissioning.

Filter	Mean Pixel Area (square arc-seconds)	Mean Pixel Area (steradian)
F090W	0.004293403755903962	1.00914010356946E-13
F115W	0.004293390754333651	1.00913704762440E-13
F140M	0.004293560394968279	1.00917692068953E-13
F150W	0.004293593015086312	1.00918458786252E-13
F158M	0.004293379993533989	1.00913451835972E-13
F200W	0.00429341540892808	1.00914284254642E-13

F277W	0.004293424689083806	1.00914502379418E-13
F356W	0.00429341834560708	1.00914353279610E-13
F380M	0.004293513635445657	1.00916593013002E-13
F430M	0.004292336159885266	1.00888917120481E-13
F444W	0.0042934269283185	1.00914555011354E-13
F480M	0.004293046386055218	1.00905610582160E-13

The estimated mean pixel area pre-flight was 0.004330336 square arc-seconds. The above values are all slightly smaller than this.

4.0 Data reduction

The initial data reduction was carried out using the 25 May 2022 version of the JWST data reduction pipeline, version number '1.5.3a1.dev1+g5269a9b'. This is not one of the formal releases but is a "snapshot" version of the pipeline as it was on the date above. The data were reduced using the reference files in the Calibration Reference Data System (CRDS) at the date when the data files were downloaded from the Barbara A. Mikulski Archive for Space Telescopes (https://mast.stsci.edu/). All the observations were later re-reduced using the reference files as of 4 July 2022, after revised imaging flat fields had been added to the system and using the 23 June 2022 version of the data reduction pipeline, version '1.5.4.dev8+g1ab10bd'. There were some changes in the level 1 pipeline in the meantime, specifically in the jump detection step, that can cause issues in the NIRISS data reductions. However, these issues usually appear when pixels saturate up the ramp, and for the standard star observations we were careful to avoid this. A comparison of the outputs from the two different pipeline versions shows that in a small number of cases where the ramp length is 3 groups and the signal level is high enough for some charge migration to take place then there may be issues with the jump detection as well. Only one observation was affected by this, the measurements of LDS 749B in F115W with the SUB356 sub-array. For that one specific case an older pipeline version from April was used in the reductions rather than the May or June versions listed above.

4.1 Frame Time Issue for SUB64

Some of the observations were taken in the SUB64 calibration sub-array, the smallest one available for NIRISS. Observations in the NIS-011a program to compare the count rates determined in full frame imaging and in each of the available sub-arrays showed a count rate discrepancy in the SUB64 case, with the output photometry for the stars in the astrometric field being smaller by a factor of 0.914. This is shown in Figure 1 below. This appeared to be an issue with the frame time assigned to the SUB64 observations because the discrepancy appears to be independent of the brightness of the source under consideration. After some investigation by Eddie Bergeron and Julia Zhou it was discovered that for NIRISS the frame time assumed, 0.05016 seconds, was instead 0.04550 seconds because the sub-arrays of size 64 pixels or less in both x and y use an

FGS-like configuration rather than the normal configuration for the near-infrared instruments. The ratio of these frame times, 0.907, is close to the ratio of 0.914 relating the SUB64 signal to the signal in all the other sub-arrays. Although the nominal uncertainty in the best-fit slope is much smaller than this 0.7% difference, the individual points in Figure 1 have uncertainties of order 1% so the greater accuracy calculated for the slope fit is probably not real. Hence, we assume that this discrepancy simply reflects the wrong frame time and does not indicate any other issue in the observations in this sub-array.

In the initial reductions and analysis those observations taken in the SUB64 configuration were wrong by this factor of 0.907 noted in the previous paragraph. To correct this the TFRAME header keyword values were manually changed from 0.05016 to 0.04550 in the raw data files and the TGROUP header keyword for NISRAPID or NIS exposures was changed from 0.05016 or 0.20064 to 0.04550 or 0.18200 respectively, and then the reduction was redone. This affects the observations in filters F090W, F115W, and F200W for LDS 749B. A change in the NIRISS subarray definition file in the OPSSOC PRD was made on 21 June 2022 to fix this issue, so all subsequent observations with this sub-array have the correct frame time.

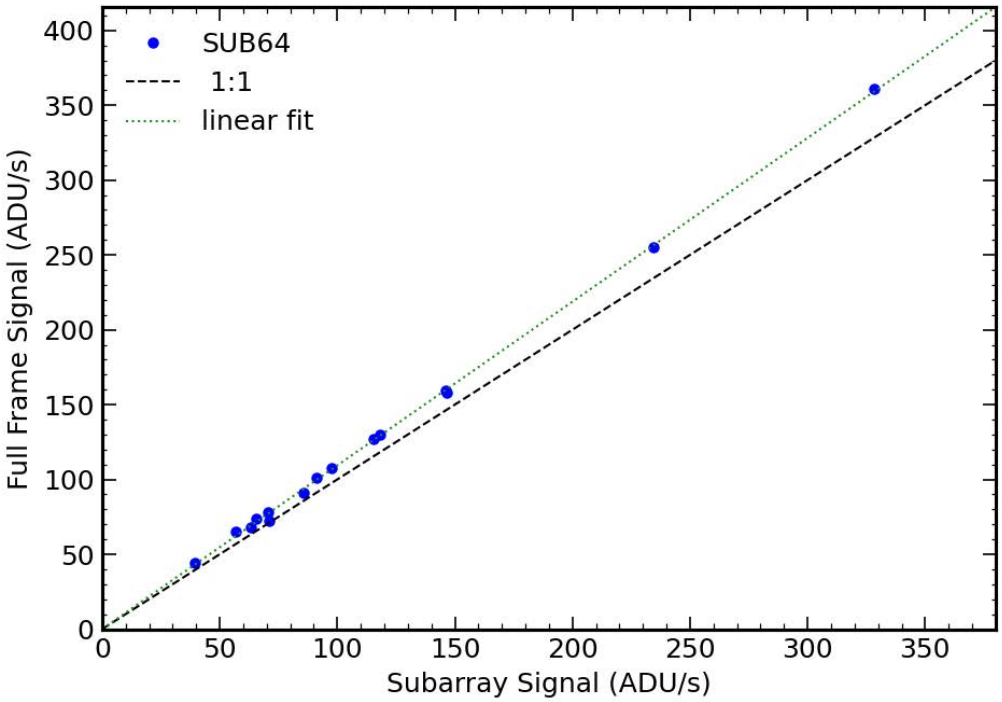

Figure 1: Comparison of the point source signal in the full frame image and that in the SUB64 image of the same field. The dotted line shows the best linear fit, which does not match the dashed 1:1 line. The observations used here are from NIS-011a.

This wrong frame time issue also affects the commissioning acquisition images. These are the only cases of 64×64 pixel sub-array exposures with NIS read-out that we have. Where measurements can be compared to exposures in other sub-arrays, these acquisition exposures also are seen to have the same frame time issue. This is what is expected since the frame time is set by the ASIC read properties with no reference to where a sub-array is located on the detector.
As far as the author knows the raw data files for the SUB64 or acquisition observations in the JWST archive were not corrected for this error in the frame times for exposures taken prior to the PRD revision, so the data reduction products are incorrect for such observations prior to the change of the DMS software.

4.2 Available Photometric Observations

Table 2 lists the full set of available photometric calibration observations for NIRISS imaging during commissioning in all programs. All of these observations were reduced in the same way as far as possible. The "regular" imaging photometry measurements in programs 01080 and 01094 use a two-point dither pattern per observation. The acquisition images use a series of 4 exposures at different positions within the acquisition sub-array, all of which are measured as a group to determine the photometric scaling factor.

Table 2: Photometric standard star observations in commissioning.

Program	Observation(s)	Target	Comments
01080	6	GSPC P177-D	Long wavelength filters F227W, F356W, F444W, and F480M
	7	WD 1057+719	Wider filters F090W to F356W
01091	1, 2	BD+60°1753	Acquisition, F480M
01094	1	LDS 749B	Normal imaging, with a variety of sub-array configurations per filter for cross-comparison. First epoch.
	2	GSPC P330-E	SUB80 imaging/NRM observations, and a single full frame NRM F480M exposure. First epoch.
	3	LDS 749B	Second epoch, duplicate observation
	4	GSPC P330-E	Second epoch, duplicate observation

4.3 Reduction Process

The reductions were done using a combination of the interactive program *imaging_photometry.py* and the non-interactive program *reduce_file_set.py*. Both codes are found in the NIS-020 part of the NIRISS commissioning reduction codes found at https://github.com/spacetelescope/niriss-commissioning/nis_comm/nis-020. A few of the individual exposures were reduced interactively to get some idea of the proper values for the parameters of interest, and then a parameter file for the *reduce_file_set.py* program was produced with these values. This worked for the NIS-020 program, although all the

early photometric observations needed to be reduced manually because they lack a proper world coordinate system (WCS) and so cannot be reduced in the automated program which depends on the WCS values to locate the correct source between dithers. The general procedure is to copy a group of '_cal' images for a single source into a directory, find the source in the first image of the set (as this is an input in the parameter file) after which the automatic version was run with a specific set of parameters in the file. This was done for both epochs and both sources in the NIS-020/01094 program.

For each of the 206 photometric images taken under programs 01080, 01091, and 01094 in commissioning the following reduction steps were taken:

1. The raw data file was reduced through the level 1 data reduction pipeline in the standard way;
2. The resulting _rate.fits file was run through the assign_wcs, flatfield, and photom steps of the imaging level 2 data reduction pipeline to produce an output _cal.fits file;
3. Each individual file was then reduced in the imaging_photometry.py code in a uniform manner, by hand, the steps used being:
    a. The input _cal.fits file was returned to a rate image by dividing by the PHOTMJSR value in the header;
    b. Any image pixels with ramp slope values below a negative threshold, set from the histogram of pixel values near 0.0, were masked out to the threshold value;
    c. Any pixels seen in the image with anomalously large ramp slopes were masked out by hand in those cases where the reduction was manual, otherwise only pixels with the DO_NOT_USE flag were masked out;
    d. The source position was determined using the PHOTUTILS IRAFStarFind algorithm, or in a few cases where this failed it was determined by the PHOTUTILS detect_sources routine;
    e. A WebbPSF model (Perrin et al., 2014) was calculated to match the sub-pixel position of the source in the image, using version 1.0.0 with 5 times oversampling and a 301×301 pixel PSF image normalized to unit total signal that is then matched to the sub-array dimensions of the observation;
    f. The PSF model image was saved to an output file;
    g. A circular aperture of radius 15 pixels and a background annulus from 15 to 21 pixels in radius were created at the source position;
    h. The source signal in the aperture was calculated using the PHOTUTILS routines, and background corrected from the signal in the background area scaled by the ratio of areas allowing for all masked pixels;
    i. The aperture correction was calculated from the PSF model image, allowing for whatever part of the normalized PSF was in the background area, and the corrected source signal was calculated;
    j. The corrected source signal, the pixel area for the filter, and the photon weighted mean flux density for the photometric standard (calculated from

the NIRISS throughput and detector response values) were used to determine the scaling factor from ADU/s to MJy/ster; and

k. The PHOTUTILS background subtraction step "Background2D" was applied to the image;
l. The source signal and scaling factor calculations were repeated after the background subtraction.

In the reduction process the images were also screened for any additional objects in the field, aside from the standard of interest. Such additional sources were generally seen at longer wavelengths, but none were close enough to the target to be of concern for the photometric measurements. The reduction failed for four F480M plus NRM exposures of low S/N where the routines could not identify the source, so there were 202 measurements in total. While these additional four cases might be done manually, with low signal it is not worth adding to the set of values.

After the reduction the values were compared to look for possible issues in individual observations. The measurements with and without the PHOTUTILS background subtraction were compared to determine the general level of uncertainty in the background correction. In most cases the measurements after the background subtraction were preferred over the initial values. The background corrected values were seen to be of order 1% higher than the non-background corrected values on the average, of the same order as the uncertainty in the individual measurements and of the differences observed between the two dither positions in each observation. The difference varies between 0.01% and about 2% over the set of observations

As an example of the processing, the following images (Figure 2 to Figure 10) show the various steps for the processing steps applied to image jw01094006001_0210h_00001_nis_cal.fits. This is an observation of the standard star LDS 749B in the F090W filter, taken on 21 May 2022. The initial data range for the image, after reversing the conversion to MJy/ster carried out in the pipeline, was –21351.717 to + 23402.6 ADU/s. Due to the few pixels with large negative slopes in the image the display does not convey as much information as one would like. Hence the need to screen out the negative values. In this particular case a threshold of –16.7 ADU/s was used for the masking of the negative slope values. The presence of negative slope values in the rate images appears to be primarily a function of ramp length, so the effect is more significant for the shorter wavelength filters where the signal per frame is larger and the ramps are correspondingly shorter. For this reason, one cannot define a generic threshold in ADU/s for the screening of the negative pxiels that works for all the photometric observations. The example here is one where the threshold is significantly more negative than is the case in the longer wavelength filters. At the longest wavelengths screening out all pixels with negative ramp slope values usually works, but that is a bad idea for the short wavelength filters. One needs to look at the background histograms on an image-by-image basis to get the best screening of the negative pixels. This cannot be automated in the *reduce_file_set.py* code.

After background subtraction the image range was from −18.8 to +23400.3 ADU/s in this particular case. The background images from the PHOTUTILS Background2D image often show structure, particularly left to right in the images although there is significant variation over the set of filters with the fitted background being quite flat in some cases. In this case, the background image range is −2.38 to +3.48 ADU/s. As it turns out, the conversion value after the background fitting step has been done is not very sensitive to the threshold for screening the negative values in the original image, and generally the background images that come from the fitting have small positive values over the region where the source is found. The background fitting and removal is one of the main sources of uncertainty in the photometric measurements. In general, the background fitting and removal seems to work better for the larger SUB256 and SUB128 sub-arrays than it does for the SUB64 sub-array even then the PSF is very compact. Possibly this is just a result of having more pixels to work with in the background fitting in the larger sub-arrays.

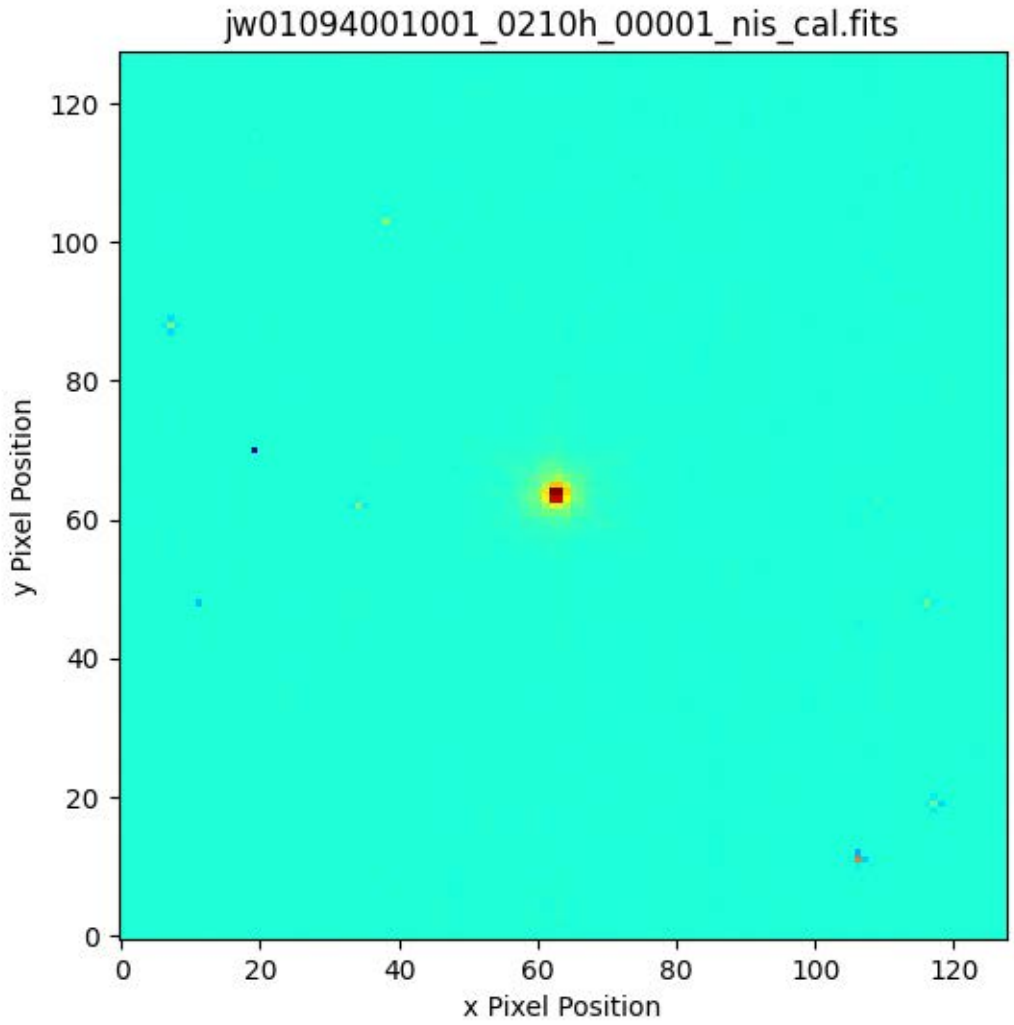

Figure 2: The raw (flat-fielded) rate image for observation jw01094001001_0210h_00001_nis_cal.fits, converted back to ADU/s from the flat-fielded, calibrated image. The image is shown on a logarithmic scale from a minimum of –292.23 ADU/s to a maximum of + 23402.6 ADU/s.

4.4 Processing Issues

There were a few specific exposures where there were unusual issues that needed to be handled by special means. The F115W exposures for LDS 749B in SUB256 were the shortest ramps of the set of observations, 3 frames long, and suffered from some charge migration from the peak pixel to the adjacent pixels. In the versions of the data reduction pipeline prior to roughly 6 May 2022 this was not an issue, but changes to the jump detection step which were made around this time caused issues for these observations in subsequent versions of the pipeline. The symptom of the issue was zero ramp slope

pixels in the core of the PSF. Files jw01094001001_0211f_0001_nis_cal.fits, jw01094001001_0211f_0002_nis_cal.fits, jw01094003001_0211f_0001_nis_cal.fits, and jw01094001001_0211f_0002_nis_cal.fits have this issue. For these particular cases the reductions needed to be redone in pipeline version '1.4.7a1.dev20+g2df8dec' from 20 April 2022 to avoid this issue. Figure 11 shows the problem.

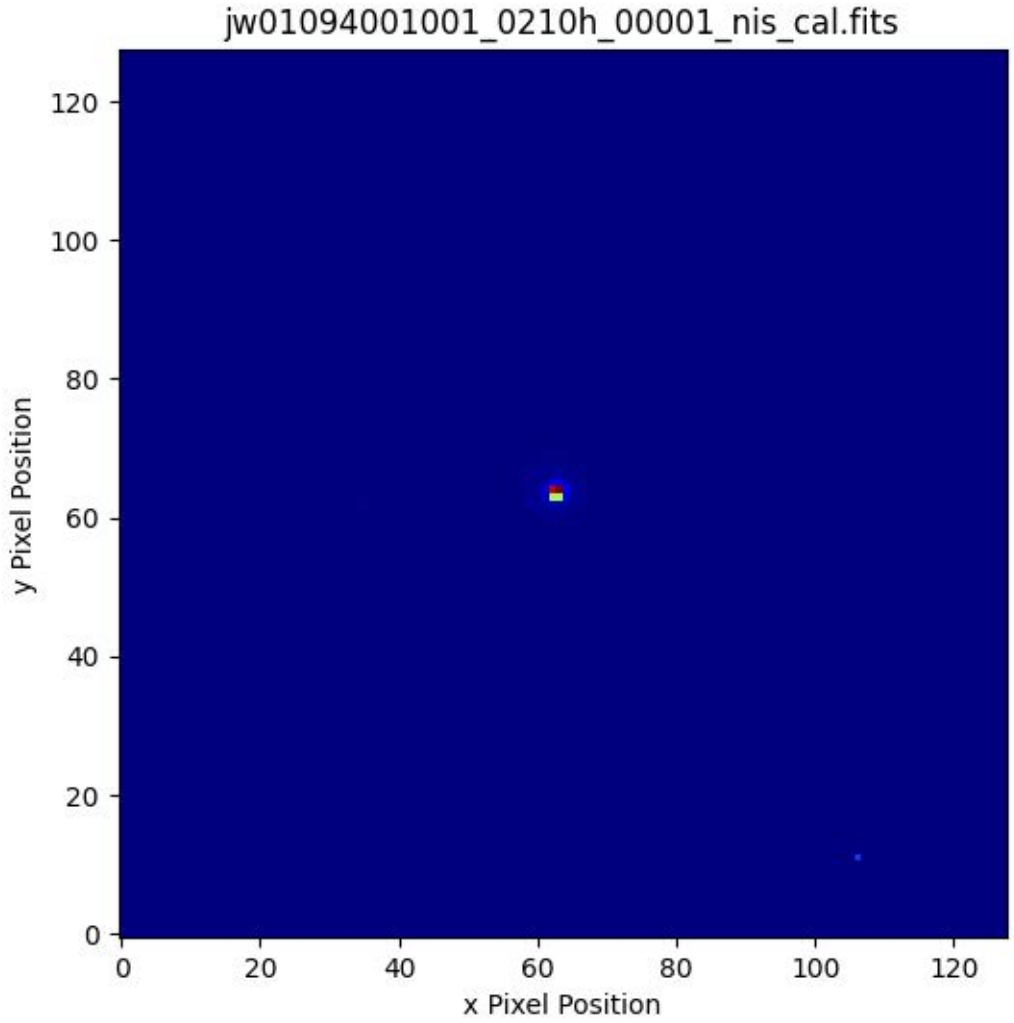

Figure 3: The same rate image as in Figure 2 after the thresholding at −16.7 ADU/s, linear scale.

A different sort of issue was seen in jw01094001001_0211h_0001_nis_cal.fits where there is a small cluster of pixels close to the PSF that have elevated values, likely due to a cosmic ray event. In this case, those pixels were simply masked off. This was the only such case seen in the photometric observations. Figure 12 shows the ramp slope image with the cluster of pixels to the right of the PSF.

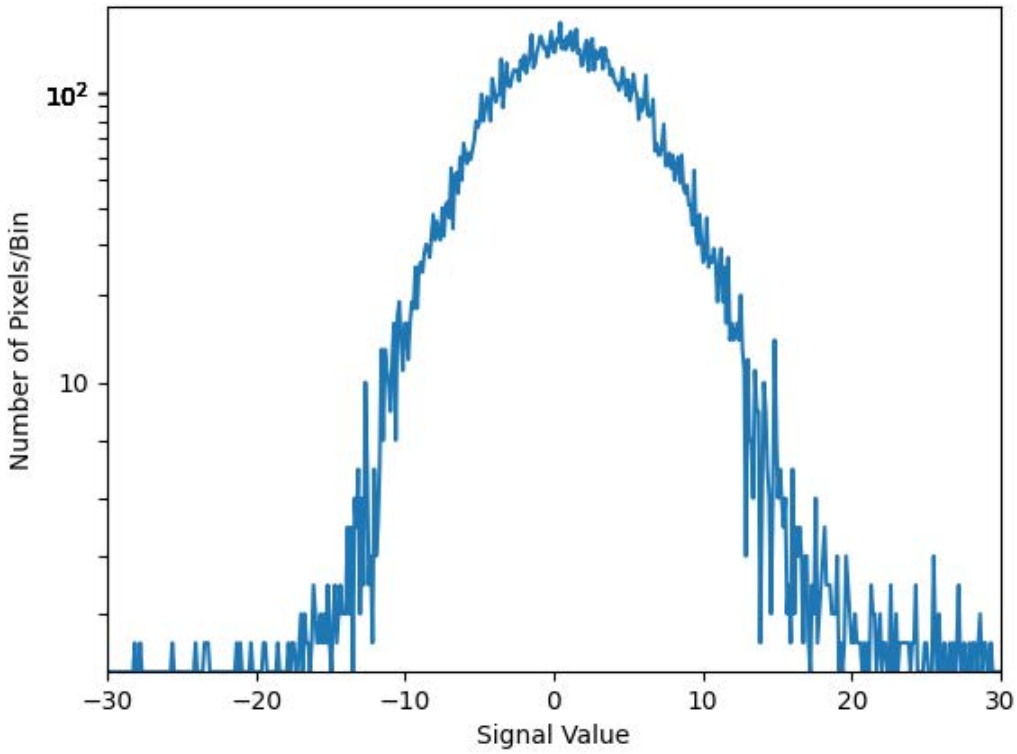

Figure 4: The histogram for the background pixels in image jw01094001001_0210h_00001_nis_rate.fits after flat-fielding. The y scale is linear up to the value of 10 and logarithmic above this value. The histogram was used to select the threshold for masking negative values. As seen above, the main component of the histogram around these signal values is approximately Gaussian in shape. In this case the minimum threshold was selected as −16.7 ADU/s.

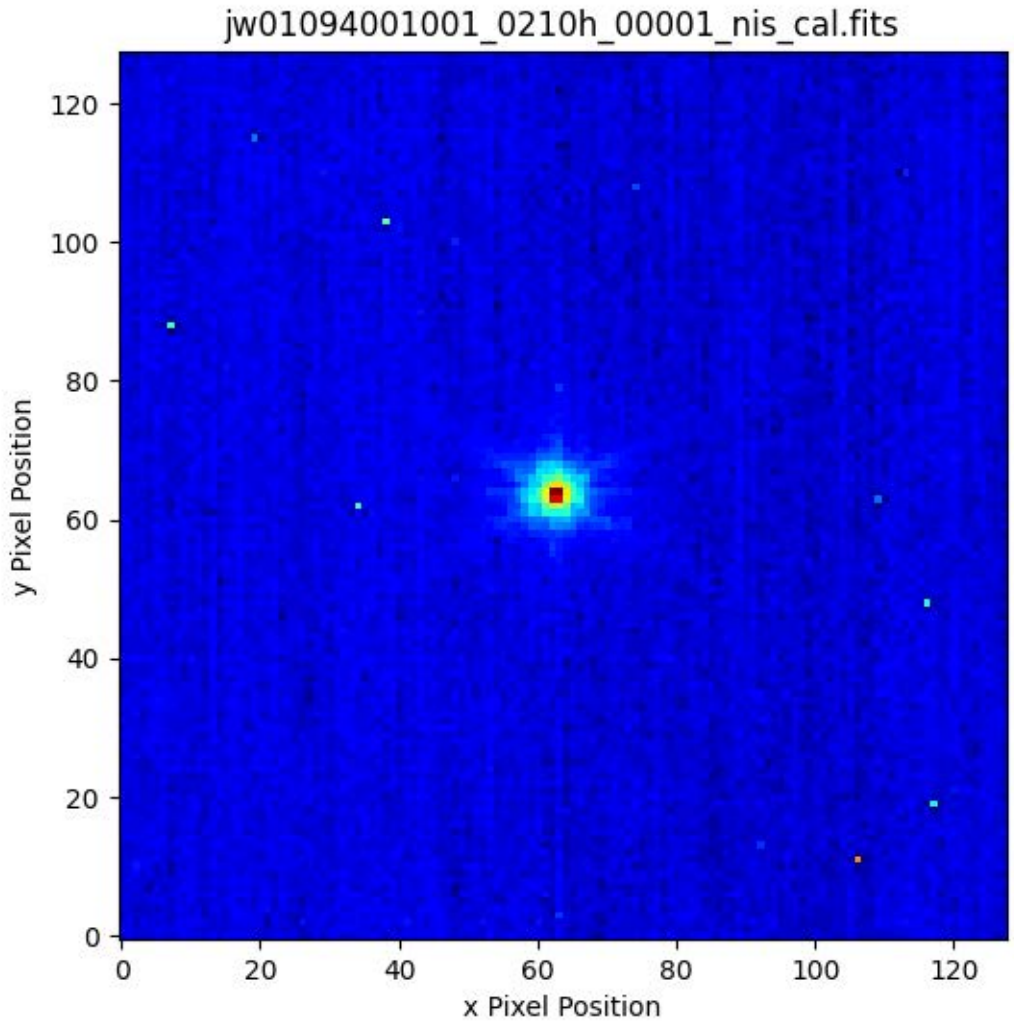

Figure 5: the same image as in Figure 3, but using a logarithmic display.

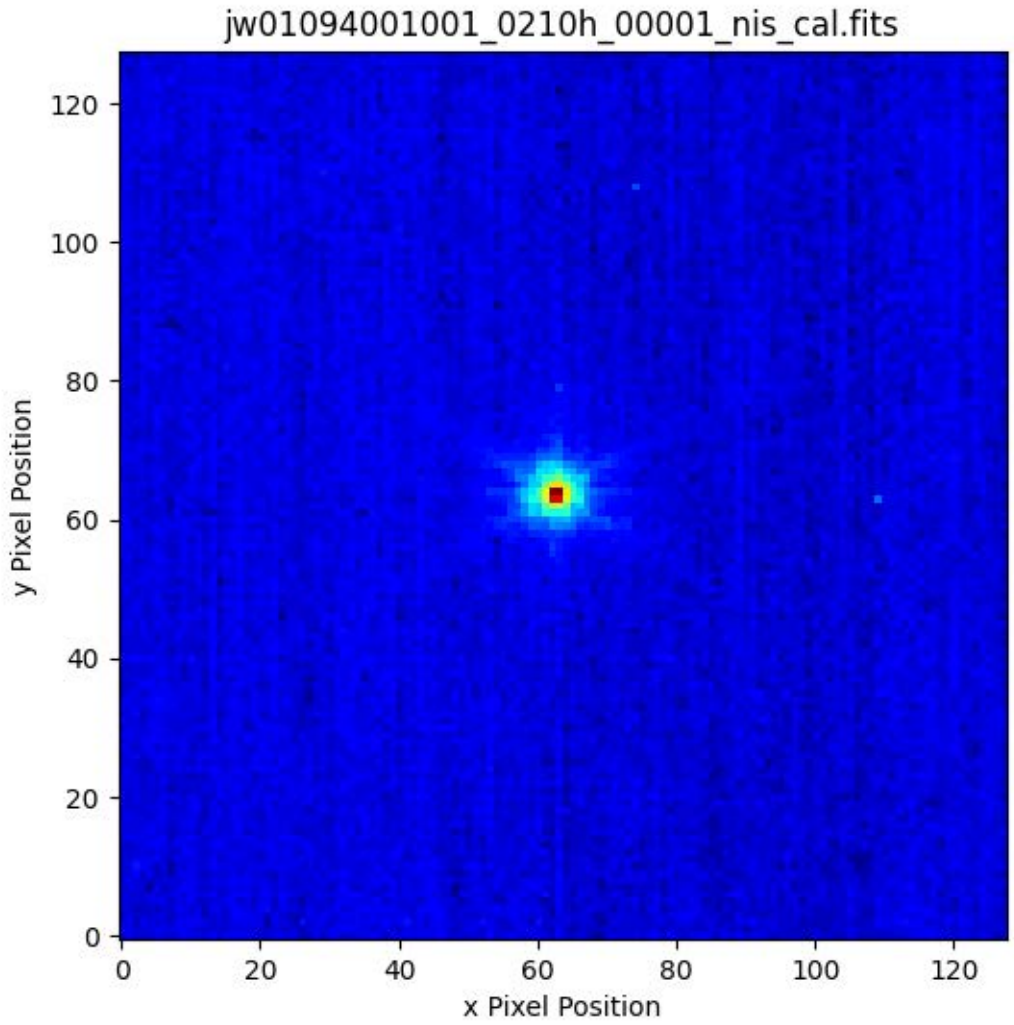

Figure 6: The rate image after the "hot" pixels are corrected.

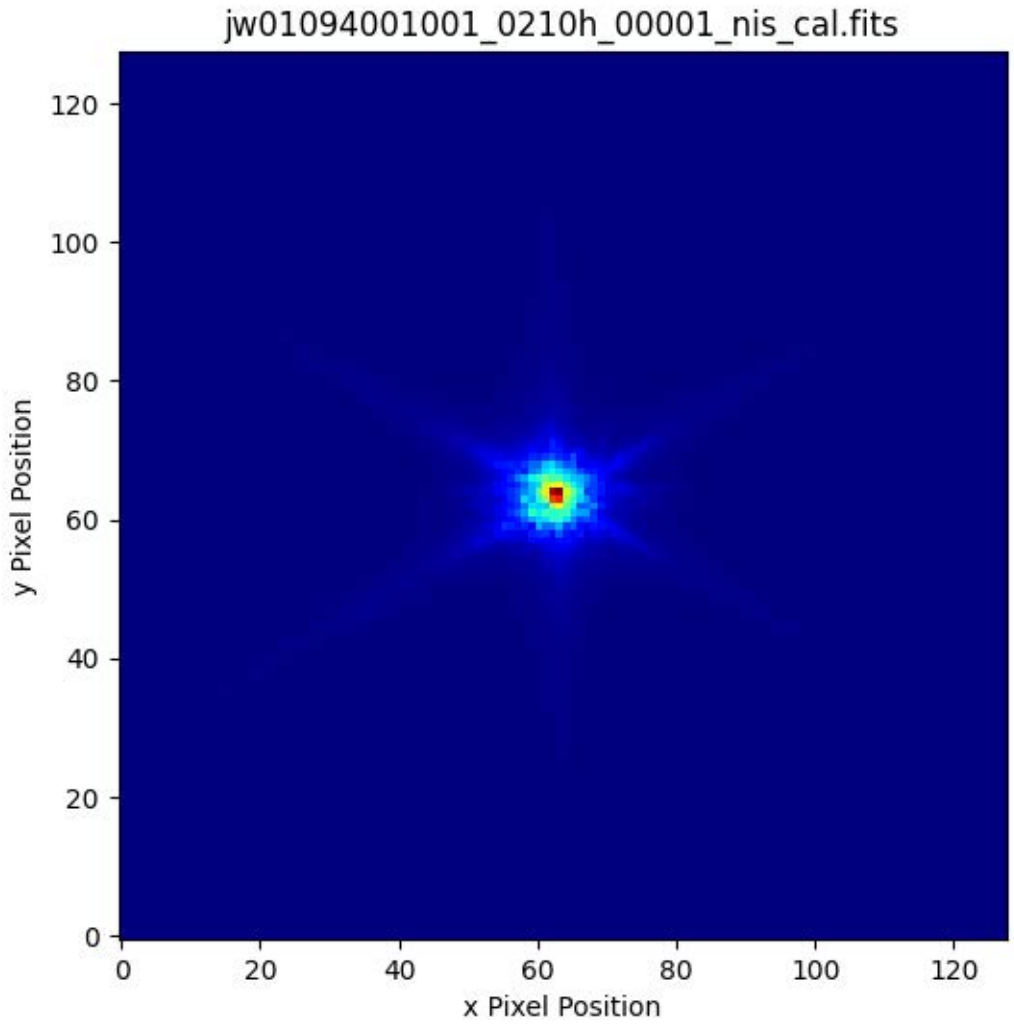

Figure 7: The PSF model image from WebbPSF for observation jw01094001001_210h.

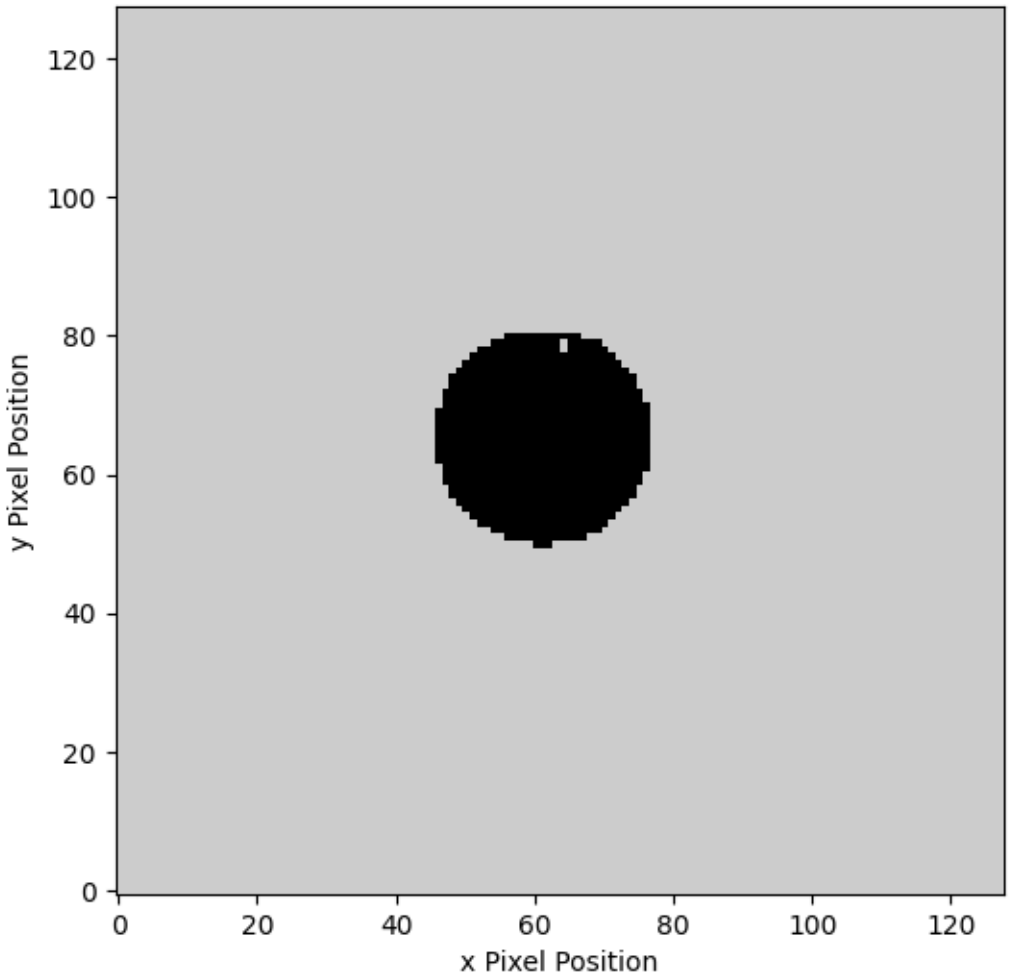

Figure 8: The source mask for the image; black pixels are selected and grey pixels are not.

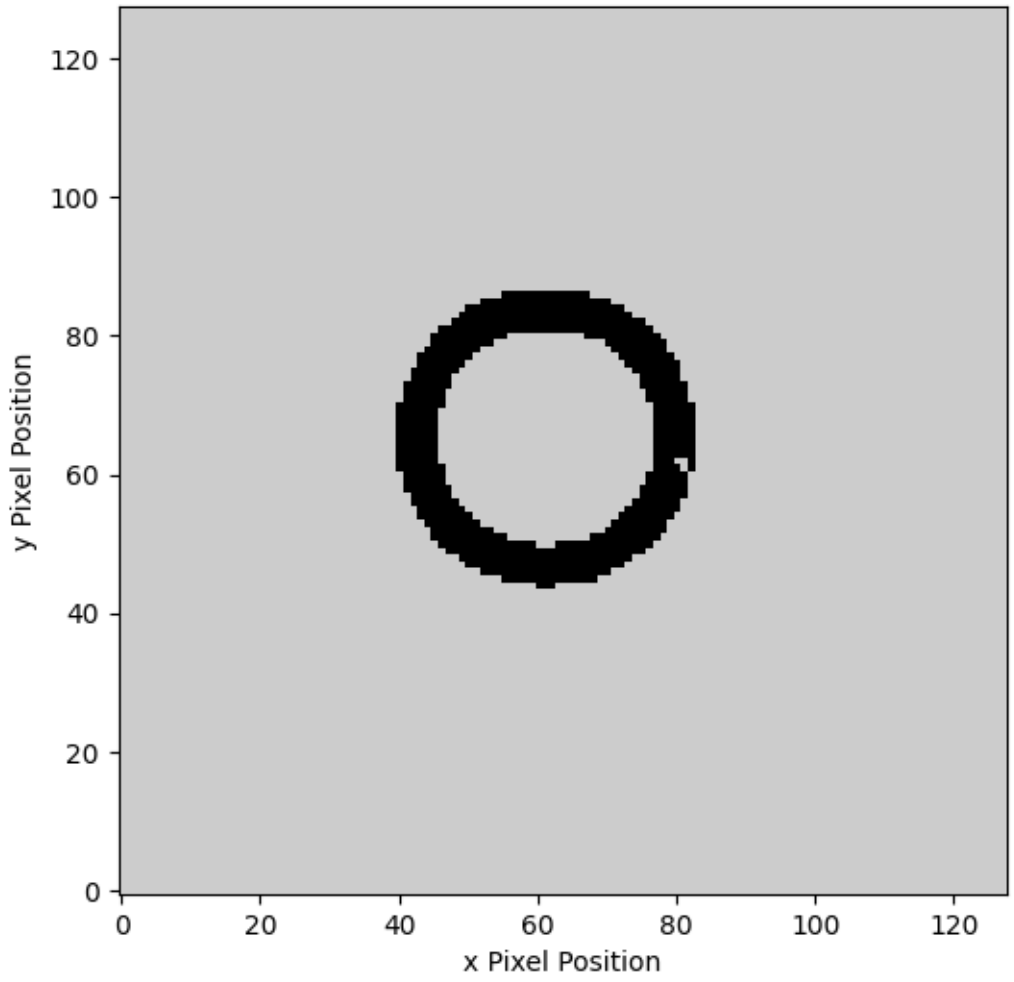

Figure 9: The background mask for the image, black pixels are selected and grep pixels are not.

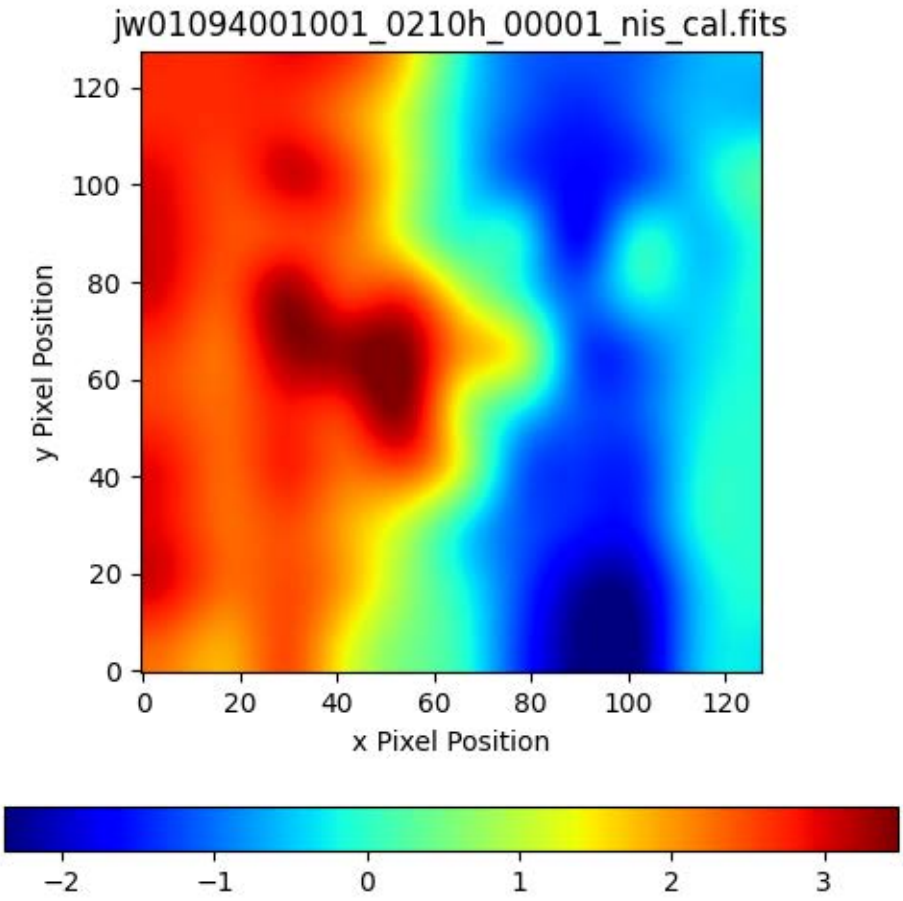

Figure 10: The output of the PHOTUTILS Background2D step for observation jw01094001001_0210h, in linear scale. One sees the typical predominantly left to right variation in the background. The values are in ADU/s units.

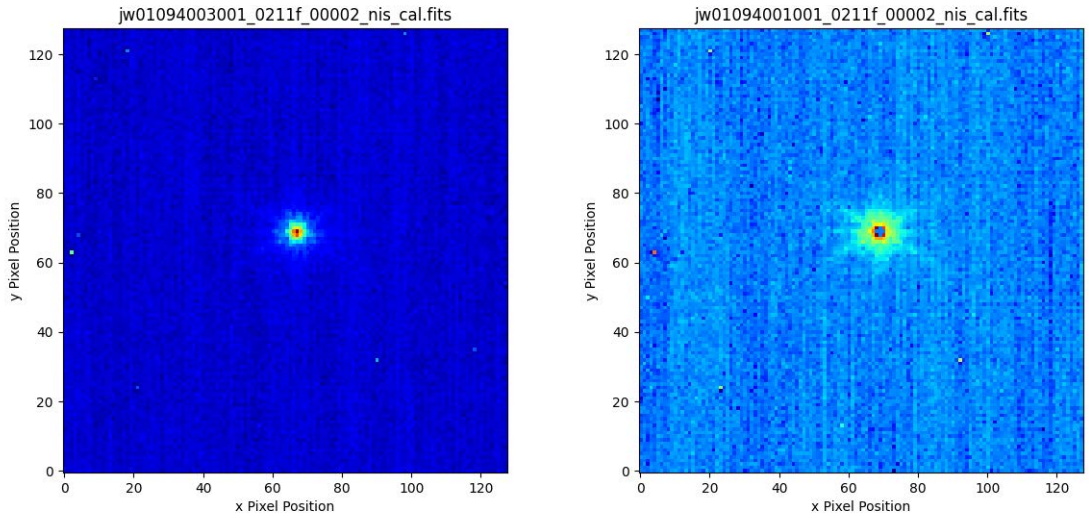

Figure 11: Illustration of the charge migration effect. The left image shows the output _cal.fits file reduced in the pipeline version from April 20, 2022, and the right image shows the output from the pipeline version from 23 June, 2022. The five pixels in the core, the peak pixel and the four immediately adjacent pixels, all have zero slope values in the right-hand image from having samples rejected in the jump detection step of the pipeline. Examination of the raw data shows that all these pixels have reasonable ramp data but that the third and last sample is affected by charge migration from the centre pixel to the four adjacent pixels which cause all the ramps to show non-linearity.

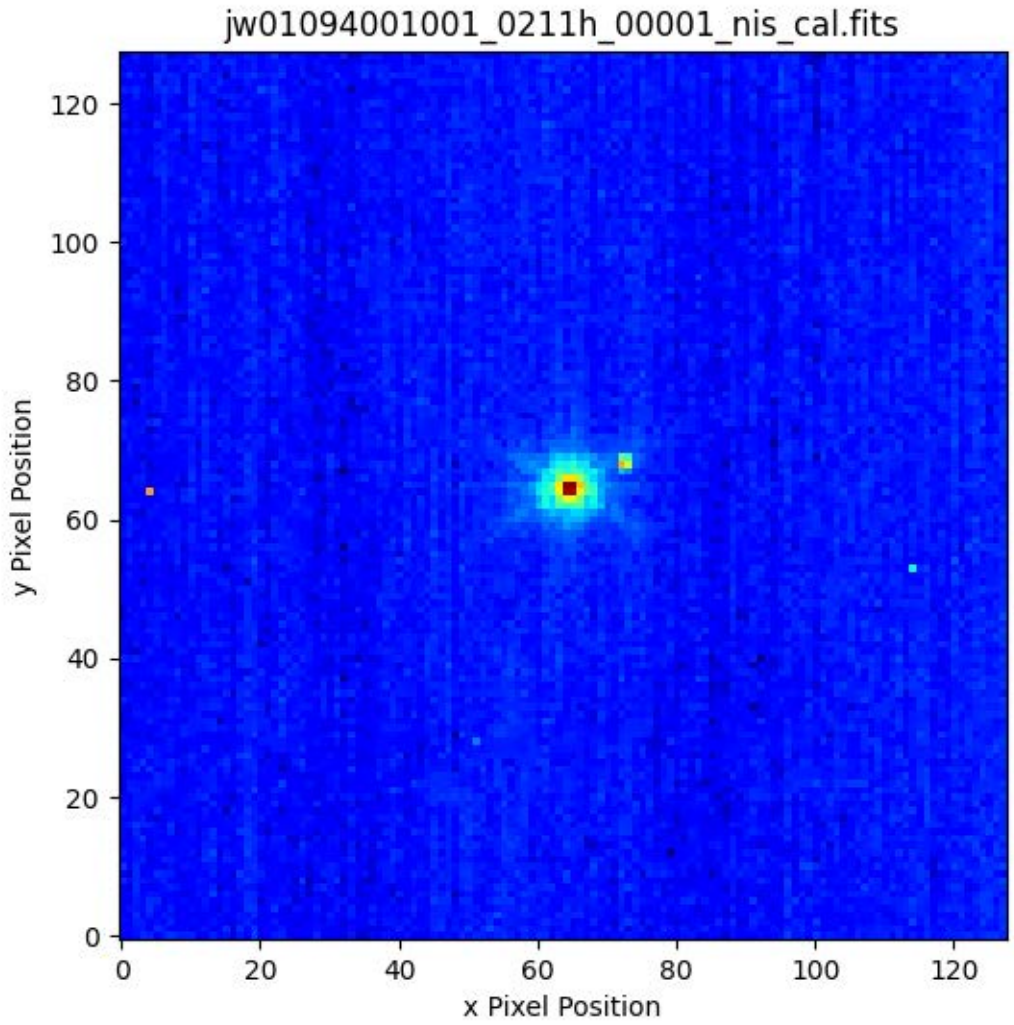

Figure 12: The rate image from jw01094001001_0211f_00001_nis_cal.fits, showing an anomalous signal from pixels just to the upper-right of the PSF. This is not seen in any other image from this source and appears to be due to a cosmic ray hit on the detector during the integration.

4.5 Background Subtraction

As noted above the PHOTUTILS Background2D routine was applied to all the images, and this produces a small correction to the photometry values. Examination of the background images produced by this routine shows that there is a wide variation in the results that seems to be somewhat wavelength dependent. The background images tend to show left-to-right structure in the images for the shorter wavelength filters. The background image has some tendency to flatten out for the longer wavelength filters, but this is not always the case. Figure 13 and Figure 14 show the magnitude of the correction. The mean ratio of the background corrected value and the raw value comes

out as 1.006 with a standard deviation of 0.007, but the largest value is 1.038 and the distribution is somewhat skewed rather than being approximately Gaussian in form. It appears that the background subtraction routine Background2D produces results that differ as a function of the sub-array size, with larger corrections when the image size is 64×64 pixels and smaller corrections as the sub-array becomes larger.

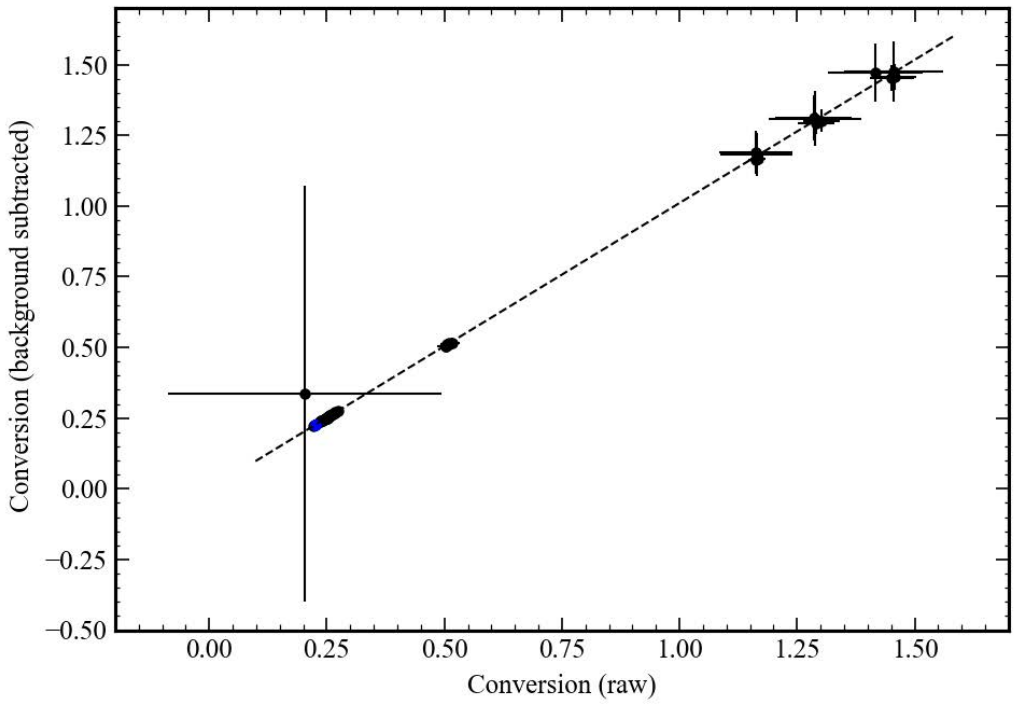

Figure 13: Comparison of the raw and background corrected conversion values for the first epoch observations of LDS 749B, with a best-fit line overplotted. The blue point shows the April pipeline version reduction value for the black point at left with the very large uncertainties, which is for image 0211f where the jump detection produced the spurious zero values in the core of the PSF. The best fit line has slope 1.0126 and intercept −0.0023.

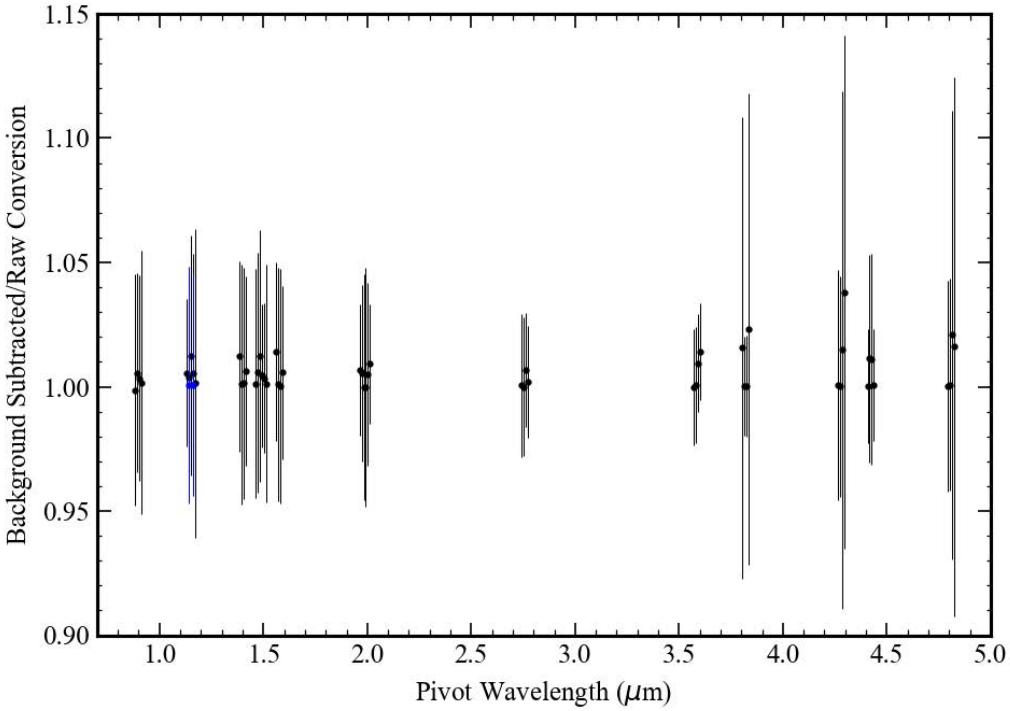

Figure 14: A plot of the background corrected conversion to raw conversion ratio as a function of the pivot wavelength of the filter for the first epoch observations of LDS 749B. The two blue points are from the 0211f observation which were reduced in the April pipeline version to avoid the jump detection issue. The wavelength values have been slightly offset from point to point.

5.0 Photometric Values

The measured values for the conversion value are listed below.

```
# Source   Filter  Value   Uncertainty    Filename
#                (MJy/ster)/(ADU/s)
GSPC P177-D F480M  1.1971  0.0164 jw01080006001_02101_00001_nis_cal.fits
GSPC P177-D F480M  1.1951  0.0166 jw01080006001_02101_00002_nis_cal.fits
GSPC P177-D F356W  0.2185  0.0032 jw01080006001_02103_00001_nis_cal.fits
GSPC P177-D F356W  0.2200  0.0031 jw01080006001_02103_00002_nis_cal.fits
GSPC P177-D F444W  0.2367  0.0026 jw01080006001_02105_00001_nis_cal.fits
GSPC P177-D F444W  0.2359  0.0027 jw01080006001_02105_00002_nis_cal.fits
GSPC P177-D F277W  0.2384  0.0057 jw01080006001_02107_00001_nis_cal.fits
GSPC P177-D F277W  0.2395  0.0057 jw01080006001_02107_00002_nis_cal.fits
PG 1057+719 F277W  0.2436  0.0035 jw01080007001_02101_00001_nis_cal.fits
PG 1057+719 F277W  0.2450  0.0035 jw01080007001_02101_00002_nis_cal.fits
PG 1057+719 F356W  0.2257  0.0036 jw01080007001_02103_00001_nis_cal.fits
PG 1057+719 F356W  0.2254  0.0037 jw01080007001_02103_00002_nis_cal.fits
PG 1057+719 F090W  0.2470  0.0070 jw01080007001_02105_00001_nis_cal.fits
PG 1057+719 F090W  0.2482  0.0068 jw01080007001_02105_00002_nis_cal.fits
PG 1057+719 F115W  0.2266  0.0064 jw01080007001_02107_00001_nis_cal.fits
PG 1057+719 F115W  0.2274  0.0064 jw01080007001_02107_00002_nis_cal.fits
PG 1057+719 F150W  0.2495  0.0054 jw01080007001_02109_00001_nis_cal.fits
PG 1057+719 F150W  0.2508  0.0052 jw01080007001_02109_00002_nis_cal.fits
```

```
PG 1057+719 F200W  0.2563  0.0044 jw01080007001_0210b_00001_nis_cal.fits
PG 1057+719 F200W  0.2569  0.0044 jw01080007001_0210b_00002_nis_cal.fits
BD+60 1753  F480M  1.2311  0.0644 jw01091001001_02101_00001_nis_cal.fits
BD+60 1753  F480M  1.2522  0.0622 jw01091001001_02101_00001_nis_cal.fits
BD+60 1753  F480M  1.2050  0.0625 jw01091001001_02101_00002_nis_cal.fits
BD+60 1753  F480M  1.2242  0.0612 jw01091001001_02101_00002_nis_cal.fits
BD+60 1753  F480M  1.2070  0.0606 jw01091001001_02101_00003_nis_cal.fits
BD+60 1753  F480M  1.2200  0.0594 jw01091001001_02101_00003_nis_cal.fits
BD+60 1753  F480M  1.2124  0.0601 jw01091001001_02101_00004_nis_cal.fits
BD+60 1753  F480M  1.2307  0.0584 jw01091001001_02101_00004_nis_cal.fits
BD+60 1753  F480M  1.2219  0.0633 jw01091002001_02101_00001-seg001_nis_cal.fits
BD+60 1753  F480M  1.2309  0.0631 jw01091002001_02101_00001-seg001_nis_cal.fits
BD+60 1753  F480M  1.2185  0.0606 jw01091002001_02101_00002-seg001_nis_cal.fits
BD+60 1753  F480M  1.2310  0.0602 jw01091002001_02101_00002-seg001_nis_cal.fits
BD+60 1753  F480M  1.2002  0.0631 jw01091002001_02101_00003-seg001_nis_cal.fits
BD+60 1753  F480M  1.2184  0.0615 jw01091002001_02101_00003-seg001_nis_cal.fits
BD+60 1753  F480M  1.1884  0.0614 jw01091002001_02101_00004-seg001_nis_cal.fits
BD+60 1753  F480M  1.2064  0.0597 jw01091002001_02101_00004-seg001_nis_cal.fits
# NIS 020 epoch 1
LAWD 87     F115W  0.2221  0.0050 jw01094001001_02101_00001_nis_cal.fits
LAWD 87     F115W  0.2268  0.0047 jw01094001001_02101_00002_nis_cal.fits
LAWD 87     F150W  0.2505  0.0052 jw01094001001_02103_00001_nis_cal.fits
LAWD 87     F150W  0.2543  0.0051 jw01094001001_02103_00002_nis_cal.fits
LAWD 87     F200W  0.2727  0.0050 jw01094001001_02105_00001_nis_cal.fits
LAWD 87     F200W  0.2635  0.0044 jw01094001001_02105_00002_nis_cal.fits
LAWD 87     F200W  0.2641  0.0067 jw01094001001_02107_00001_nis_cal.fits
LAWD 87     F200W  0.2706  0.0067 jw01094001001_02107_00002_nis_cal.fits
LAWD 87     F150W  0.2548  0.0088 jw01094001001_02109_00001_nis_cal.fits
LAWD 87     F150W  0.2541  0.0085 jw01094001001_02109_00002_nis_cal.fits
LAWD 87     F140M  0.5180  0.0136 jw01094001001_0210b_00001_nis_cal.fits
LAWD 87     F140M  0.5148  0.0135 jw01094001001_0210b_00002_nis_cal.fits
LAWD 87     F158M  0.5143  0.0125 jw01094001001_0210d_00001_nis_cal.fits
LAWD 87     F158M  0.5073  0.0122 jw01094001001_0210d_00002_nis_cal.fits
LAWD 87     F115W  0.2316  0.0076 jw01094001001_0210f_00001_nis_cal.fits
LAWD 87     F115W  0.2366  0.0079 jw01094001001_0210f_00002_nis_cal.fits
LAWD 87     F090W  0.2464  0.0068 jw01094001001_0210h_00001_nis_cal.fits
LAWD 87     F090W  0.2488  0.0072 jw01094001001_0210h_00002_nis_cal.fits
LAWD 87     F480M  1.3160  0.0807 jw01094001001_0210j_00001_nis_cal.fits
LAWD 87     F480M  1.3133  0.0978 jw01094001001_0210j_00002_nis_cal.fits
LAWD 87     F380M  1.1918  0.0756 jw01094001001_0210l_00001_nis_cal.fits
LAWD 87     F380M  1.1854  0.0753 jw01094001001_0210l_00002_nis_cal.fits
LAWD 87     F430M  1.4807  0.1067 jw01094001001_0210n_00001_nis_cal.fits
LAWD 87     F430M  1.4749  0.1026 jw01094001001_0210n_00002_nis_cal.fits
LAWD 87     F356W  0.2401  0.0033 jw01094001001_0210p_00001_nis_cal.fits
LAWD 87     F356W  0.2406  0.0033 jw01094001001_0210p_00002_nis_cal.fits
LAWD 87     F444W  0.2595  0.0075 jw01094001001_0210r_00001_nis_cal.fits
LAWD 87     F444W  0.2585  0.0076 jw01094001001_0210r_00002_nis_cal.fits
LAWD 87     F277W  0.2553  0.0041 jw01094001001_0210t_00001_nis_cal.fits
LAWD 87     F277W  0.2557  0.0041 jw01094001001_0210t_00002_nis_cal.fits
LAWD 87     F277W  0.2536  0.0051 jw01094001001_0210v_00001_nis_cal.fits
LAWD 87     F277W  0.2503  0.0051 jw01094001001_0210v_00002_nis_cal.fits
LAWD 87     F444W  0.2558  0.0041 jw01094001001_0210x_00001_nis_cal.fits
LAWD 87     F444W  0.2551  0.0041 jw01094001001_0210x_00002_nis_cal.fits
LAWD 87     F356W  0.2365  0.0039 jw01094001001_0210z_00001_nis_cal.fits
LAWD 87     F356W  0.2361  0.0039 jw01094001001_0210z_00002_nis_cal.fits
LAWD 87     F430M  1.4609  0.0458 jw01094001001_02111_00001_nis_cal.fits
LAWD 87     F430M  1.4562  0.0475 jw01094001001_02111_00002_nis_cal.fits
LAWD 87     F380M  1.1704  0.0166 jw01094001001_02113_00001_nis_cal.fits
LAWD 87     F380M  1.1658  0.0168 jw01094001001_02113_00002_nis_cal.fits
LAWD 87     F480M  1.3061  0.0393 jw01094001001_02115_00001_nis_cal.fits
LAWD 87     F480M  1.2966  0.0389 jw01094001001_02115_00002_nis_cal.fits
```

```
LAWD 87     F200W  0.2637  0.0089 jw01094001001_02117_00001_nis_cal.fits
LAWD 87     F200W  0.2633  0.0085 jw01094001001_02117_00002_nis_cal.fits
LAWD 87     F150W  0.2512  0.0085 jw01094001001_02119_00001_nis_cal.fits
LAWD 87     F150W  0.2538  0.0083 jw01094001001_02119_00002_nis_cal.fits
LAWD 87     F140M  0.5182  0.0170 jw01094001001_0211b_00001_nis_cal.fits
LAWD 87     F140M  0.5117  0.0174 jw01094001001_0211b_00002_nis_cal.fits
LAWD 87     F158M  0.5044  0.0169 jw01094001001_0211d_00001_nis_cal.fits
LAWD 87     F158M  0.5037  0.0168 jw01094001001_0211d_00002_nis_cal.fits
LAWD 87     F115W  0.2285  0.0099 jw01094001001_0211f_00001_nis_cal.fits
LAWD 87     F115W  0.2155  0.0173 jw01094001001_0211f_00002_nis_cal.fits
LAWD 87     F090W  0.2321  0.0084 jw01094001001_0211h_00001_nis_cal.fits
LAWD 87     F090W  0.2511  0.0083 jw01094001001_0211h_00002_nis_cal.fits
LAWD 87     F444W  0.2742  0.0074 jw01094001002_02101_00001_nis_cal.fits
LAWD 87     F444W  0.2507  0.0063 jw01094001002_02101_00002_nis_cal.fits
LAWD 87     F356W  0.2605  0.0080 jw01094001002_02103_00001_nis_cal.fits
LAWD 87     F356W  0.2363  0.0065 jw01094001002_02103_00002_nis_cal.fits
LAWD 87     F430M  1.5727  0.0378 jw01094001002_02105_00001_nis_cal.fits
LAWD 87     F430M  1.4315  0.0316 jw01094001002_02105_00002_nis_cal.fits
LAWD 87     F380M  1.3084  0.0415 jw01094001002_02107_00001_nis_cal.fits
LAWD 87     F380M  1.1449  0.0318 jw01094001002_02107_00002_nis_cal.fits
LAWD 87     F480M  1.4299  0.0343 jw01094001002_02109_00001_nis_cal.fits
LAWD 87     F480M  1.2802  0.0281 jw01094001002_02109_00002_nis_cal.fits
GSPC P330-E F480M  1.2122  0.0801 jw01094002001_02101_00001_nis_cal.fits
GSPC P330-E F480M  1.2193  0.0768 jw01094002001_02101_00002_nis_cal.fits
GSPC P330-E F480M  1.2571  0.0729 jw01094002001_02101_00003_nis_cal.fits
GSPC P330-E F480M  1.2871  0.0765 jw01094002001_02101_00004_nis_cal.fits
GSPC P330-E F480M  1.2450  0.0208 jw01094002001_03102_00001_nis_cal.fits
GSPC P330-E F480M  1.2396  0.0198 jw01094002001_03102_00002_nis_cal.fits
GSPC P330-E F380M  1.1029  0.0250 jw01094002001_03104_00001_nis_cal.fits
GSPC P330-E F380M  1.1080  0.0243 jw01094002001_03104_00002_nis_cal.fits
GSPC P330-E F430M  1.3946  0.0257 jw01094002001_03106_00001_nis_cal.fits
GSPC P330-E F430M  1.3963  0.0257 jw01094002001_03106_00002_nis_cal.fits
GSPC P330-E F277W  0.2443  0.0119 jw01094002001_03108_00001_nis_cal.fits
GSPC P330-E F277W  0.2489  0.0113 jw01094002001_03108_00002_nis_cal.fits
GSPC P330-E F277W  1.7891  0.0267 jw01094002001_0310a_00001_nis_cal.fits
GSPC P330-E F277W  1.8225  0.0270 jw01094002001_0310a_00002_nis_cal.fits
GSPC P330-E F430M  9.6767  1.1197 jw01094002001_0310c_00001_nis_cal.fits
# With NRM
GSPC P330-E F430M 11.1394  1.3989 jw01094002001_0310c_00002_nis_cal.fits
GSPC P330-E F380M  8.6189  0.8846 jw01094002001_0310e_00001_nis_cal.fits
GSPC P330-E F380M  8.5359  0.9338 jw01094002001_0310e_00002_nis_cal.fits
GSPC P330-E F480M  8.8042  0.8576 jw01094002001_0310g_00001_nis_cal.fits
GSPC P330-E F480M  9.9101  1.0433 jw01094002001_0310g_00002_nis_cal.fits
# NIS 020 epoch 2
LAWD 87     F115W  0.2263  0.0053 jw01094003001_02101_00001_nis_cal.fits
LAWD 87     F115W  0.2285  0.0050 jw01094003001_02101_00002_nis_cal.fits
LAWD 87     F150W  0.2529  0.0055 jw01094003001_02103_00001_nis_cal.fits
LAWD 87     F150W  0.2558  0.0053 jw01094003001_02103_00002_nis_cal.fits
LAWD 87     F200W  0.2716  0.0052 jw01094003001_02105_00001_nis_cal.fits
LAWD 87     F200W  0.2657  0.0044 jw01094003001_02105_00002_nis_cal.fits
LAWD 87     F200W  0.2652  0.0068 jw01094003001_02107_00001_nis_cal.fits
LAWD 87     F200W  0.2710  0.0071 jw01094003001_02107_00002_nis_cal.fits
LAWD 87     F150W  0.2601  0.0085 jw01094003001_02109_00001_nis_cal.fits
LAWD 87     F150W  0.2547  0.0083 jw01094003001_02109_00002_nis_cal.fits
LAWD 87     F140M  0.5247  0.0137 jw01094003001_0210b_00001_nis_cal.fits
LAWD 87     F140M  0.5128  0.0143 jw01094003001_0210b_00002_nis_cal.fits
LAWD 87     F158M  0.5149  0.0132 jw01094003001_0210d_00001_nis_cal.fits
LAWD 87     F158M  0.5070  0.0127 jw01094003001_0210d_00002_nis_cal.fits
LAWD 87     F115W  0.2347  0.0074 jw01094003001_0210f_00001_nis_cal.fits
LAWD 87     F115W  0.2375  0.0080 jw01094003001_0210f_00002_nis_cal.fits
LAWD 87     F090W  0.2488  0.0096 jw01094003001_0210h_00001_nis_cal.fits
```

```
LAWD 87     F090W  0.2448  0.0095 jw01094003001_0210h_00002_nis_cal.fits
LAWD 87     F480M  1.2925  0.0881 jw01094003001_0210j_00001_nis_cal.fits
LAWD 87     F480M  1.3125  0.0864 jw01094003001_0210j_00002_nis_cal.fits
LAWD 87     F380M  1.2153  0.0805 jw01094003001_0210l_00001_nis_cal.fits
LAWD 87     F380M  1.1800  0.0784 jw01094003001_0210l_00002_nis_cal.fits
LAWD 87     F430M  1.4912  0.0880 jw01094003001_0210n_00001_nis_cal.fits
LAWD 87     F430M  1.5008  0.0931 jw01094003001_0210n_00002_nis_cal.fits
LAWD 87     F356W  0.2405  0.0033 jw01094003001_0210p_00001_nis_cal.fits
LAWD 87     F356W  0.2417  0.0032 jw01094003001_0210p_00002_nis_cal.fits
LAWD 87     F444W  0.2594  0.0075 jw01094003001_0210r_00001_nis_cal.fits
LAWD 87     F444W  0.2599  0.0073 jw01094003001_0210r_00002_nis_cal.fits
LAWD 87     F277W  0.2565  0.0043 jw01094003001_0210t_00001_nis_cal.fits
LAWD 87     F277W  0.2562  0.0042 jw01094003001_0210t_00002_nis_cal.fits
LAWD 87     F277W  0.2535  0.0052 jw01094003001_0210v_00001_nis_cal.fits
LAWD 87     F277W  0.2533  0.0051 jw01094003001_0210v_00002_nis_cal.fits
LAWD 87     F444W  0.2575  0.0040 jw01094003001_0210x_00001_nis_cal.fits
LAWD 87     F444W  0.2556  0.0040 jw01094003001_0210x_00002_nis_cal.fits
LAWD 87     F356W  0.2382  0.0040 jw01094003001_0210z_00001_nis_cal.fits
LAWD 87     F356W  0.2374  0.0040 jw01094003001_0210z_00002_nis_cal.fits
LAWD 87     F430M  1.4733  0.0471 jw01094003001_02111_00001_nis_cal.fits
LAWD 87     F430M  1.4600  0.0468 jw01094003001_02111_00002_nis_cal.fits
LAWD 87     F380M  1.1739  0.0173 jw01094003001_02113_00001_nis_cal.fits
LAWD 87     F380M  1.1647  0.0169 jw01094003001_02113_00002_nis_cal.fits
LAWD 87     F480M  1.3133  0.0387 jw01094003001_02115_00001_nis_cal.fits
LAWD 87     F480M  1.3003  0.0388 jw01094003001_02115_00002_nis_cal.fits
LAWD 87     F200W  0.2665  0.0088 jw01094003001_02117_00001_nis_cal.fits
LAWD 87     F200W  0.2680  0.0093 jw01094003001_02117_00002_nis_cal.fits
LAWD 87     F150W  0.2556  0.0088 jw01094003001_02119_00001_nis_cal.fits
LAWD 87     F150W  0.2524  0.0093 jw01094003001_02119_00002_nis_cal.fits
LAWD 87     F140M  0.5167  0.0186 jw01094003001_0211b_00001_nis_cal.fits
LAWD 87     F140M  0.5144  0.0183 jw01094003001_0211b_00002_nis_cal.fits
LAWD 87     F158M  0.5122  0.0173 jw01094003001_0211d_00001_nis_cal.fits
LAWD 87     F158M  0.5083  0.0183 jw01094003001_0211d_00002_nis_cal.fits
LAWD 87     F115W  0.2644  0.0100 jw01094003001_0211f_00001_nis_cal.fits
LAWD 87     F115W  0.1862  0.0143 jw01094003001_0211f_00002_nis_cal.fits
LAWD 87     F090W  0.2491  0.0092 jw01094003001_0211h_00001_nis_cal.fits
LAWD 87     F090W  0.2467  0.0099 jw01094003001_0211h_00002_nis_cal.fits
LAWD 87     F444W  0.2793  0.0078 jw01094003002_02101_00001_nis_cal.fits
LAWD 87     F444W  0.2515  0.0064 jw01094003002_02101_00002_nis_cal.fits
LAWD 87     F356W  0.2660  0.0086 jw01094003002_02103_00001_nis_cal.fits
LAWD 87     F356W  0.2475  0.0077 jw01094003002_02103_00002_nis_cal.fits
LAWD 87     F430M  1.6059  0.0389 jw01094003002_02105_00001_nis_cal.fits
LAWD 87     F430M  1.4377  0.0306 jw01094003002_02105_00002_nis_cal.fits
LAWD 87     F380M  1.3284  0.0434 jw01094003002_02107_00001_nis_cal.fits
LAWD 87     F380M  1.1514  0.0323 jw01094003002_02107_00002_nis_cal.fits
LAWD 87     F480M  1.4593  0.0348 jw01094003002_02109_00001_nis_cal.fits
LAWD 87     F480M  1.2878  0.0269 jw01094003002_02109_00002_nis_cal.fits
GSPC P330-E F480M  1.2892  0.0778 jw01094004001_02101_00001_nis_cal.fits
GSPC P330-E F480M  1.2434  0.0778 jw01094004001_02101_00002_nis_cal.fits
GSPC P330-E F480M  1.2654  0.0798 jw01094004001_02101_00003_nis_cal.fits
GSPC P330-E F480M  1.2301  0.0765 jw01094004001_02101_00004_nis_cal.fits
GSPC P330-E F480M  1.2732  0.0182 jw01094004001_03102_00001_nis_cal.fits
GSPC P330-E F480M  1.3013  0.0182 jw01094004001_03102_00002_nis_cal.fits
GSPC P330-E F380M  1.1122  0.0212 jw01094004001_03104_00001_nis_cal.fits
GSPC P330-E F380M  1.1297  0.0212 jw01094004001_03104_00002_nis_cal.fits
GSPC P330-E F430M  1.4106  0.0235 jw01094004001_03106_00001_nis_cal.fits
GSPC P330-E F430M  1.4262  0.0229 jw01094004001_03106_00002_nis_cal.fits
GSPC P330-E F277W  0.2476  0.0077 jw01094004001_03108_00001_nis_cal.fits
GSPC P330-E F277W  0.2489  0.0075 jw01094004001_03108_00002_nis_cal.fits
# With NRM
GSPC P330-E F430M 10.1642  1.1969 jw01094004001_0310a_00001_nis_cal.fits
```

```
GSPC P330-E F430M 11.5410  1.3903 jw01094004001_0310a_00002_nis_cal.fits
GSPC P330-E F380M  7.4777  0.7005 jw01094004001_0310c_00001_nis_cal.fits
GSPC P330-E F380M  8.2449  0.8241 jw01094004001_0310c_00002_nis_cal.fits
GSPC P330-E F480M  9.5122  1.0241 jw01094004001_0310e_00001_nis_cal.fits
GSPC P330-E F480M  9.4784  1.0160 jw01094004001_0310e_00002_nis_cal.fits
```

From these values the mean values per filter configuration for each source and epoch were calculated. These values are given in the next table. The wavelength values given in the table are the filter pivot wavelengths. The mean value is calculated using the sigma-clipped statistics routine from the astropy package in cases where more than 5 values are measured, and otherwise the normal mean is calculated. The standard deviation values are also either from the sigma-clipped statistics routine or the normal numpy routine, depending on the number of measurements. The uncertainties assigned to each measurement cannot be used in the averaging in the astropy sigma-clipped statistics routine, so they are also not used when the normal numpy routine was applied. In all cases the sample standard deviation is quoted as the uncertainty rather than the standard deviation in the mean.

```
#   Filter      Pupil  Wavelength     Scaling   Uncertainty
# LDS 749B Epoch 1
     CLEAR      F090W   0.902460     0.244580     0.007391
     CLEAR      F115W   1.149540     0.226848     0.006747
     CLEAR      F140M   1.404030     0.515652     0.002660
     CLEAR      F150W   1.493460     0.253114     0.001624
     CLEAR      F158M   1.582010     0.507419     0.004190
     CLEAR      F200W   1.992960     0.266312     0.003809
     F277W     CLEARP   2.764280     0.253724     0.002122
     F356W     CLEARP   3.593000     0.241680     0.008592
     F380M     CLEARP   3.825230     1.194465     0.053113
     F430M     CLEARP   4.283830     1.479465     0.044524
     F444W     CLEARP   4.427700     0.258988     0.007352
     F480M     CLEARP   4.815240     1.323678     0.048951
# LDS 749B Epoch 2
     CLEAR      F090W   0.902460     0.247343     0.001755
     CLEAR      F115W   1.149540     0.229585     0.023070
     CLEAR      F140M   1.404030     0.517139     0.004569
     CLEAR      F150W   1.493460     0.255267     0.002516
     CLEAR      F158M   1.582010     0.510594     0.003133
     CLEAR      F200W   1.992960     0.268011     0.002491
     F277W     CLEARP   2.764280     0.254875     0.001474
     F356W     CLEARP   3.593000     0.245218     0.009833
     F380M     CLEARP   3.825230     1.202303     0.059696
     F430M     CLEARP   4.283830     1.494832     0.053747
     F444W     CLEARP   4.427700     0.260533     0.008840
     F480M     CLEARP   4.815240     1.327606     0.059633
# GSPC P330-E Epoch 1
     F277W     CLEARP   2.764280     0.246622     0.002303
     F380M     CLEARP   3.825230     1.105432     0.002557
     F430M     CLEARP   4.283830     1.395456     0.000816
```

```
     F480M     CLEARP   4.815240     1.243371     0.024712
     F277W        NRM   2.764280     1.805825     0.016701
     F380M        NRM   3.825230     8.577395     0.041512
     F430M        NRM   4.283830    10.408022     0.731339
     F480M        NRM   4.815240     9.357157     0.552992
# GSPC P330-E Epoch 2
     F277W     CLEARP   2.764280     0.248208     0.000652
     F380M     CLEARP   3.825230     1.120970     0.008733
     F430M     CLEARP   4.283830     1.418371     0.007798
     F480M     CLEARP   4.815240     1.267107     0.024576
     F380M        NRM   3.825230     7.861309     0.383600
     F430M        NRM   4.283830    10.852615     0.688425
     F480M        NRM   4.815240     9.495267     0.016917
# BD+60 1753
     F480M     CLEARP   4.815240     1.223100     0.003500
# GSPC P177-D
     F277W     CLEARP   2.764280     0.238938     0.000535
     F356W     CLEARP   3.593000     0.219258     0.000732
     F444W     CLEARP   4.427700     0.236265     0.000395
     F480M     CLEARP   4.815240     1.196109     0.001025
# WD 1057+719
     CLEAR      F090W   0.902460     0.247590     0.000573
     CLEAR      F115W   1.149540     0.226954     0.000398
     CLEAR      F150W   1.493460     0.250187     0.000653
     CLEAR      F200W   1.992960     0.256605     0.000296
     F277W     CLEARP   2.764280     0.244278     0.000714
     F356W     CLEARP   3.593000     0.225556     0.000157
```

Figure 15 shows the average photometry values for the different standard stars in normal imaging. Figure 16 shows the same plot for the NRM case in the three medium-band filters. Where needed the pivot wavelength values have been slightly offset between the epoch 1 and epoch 2 observations, to make it easier to see the data points and their uncertainties. The overall mean values plotted in this Figure and used for the pipeline reference file are:

```
#   Filter      Pupil  Wavelength   Scaling   Uncertainty
     CLEAR      F090W   0.902460   0.245961    0.001382
     CLEAR      F115W   1.149540   0.228216    0.001369
     CLEAR      F140M   1.404030   0.516396    0.000744
     CLEAR      F150W   1.493460   0.254190    0.001077
     CLEAR      F158M   1.582010   0.509006    0.001588
     CLEAR      F200W   1.992960   0.267161    0.000850
     F277W     CLEARP   2.764280   0.254300    0.000576
     F356W     CLEARP   3.593000   0.243449    0.001769
     F380M     CLEARP   3.825230   1.198384    0.003919
     F430M     CLEARP   4.283830   1.487148    0.007683
     F444W     CLEARP   4.427700   0.259761    0.000773
     F480M     CLEARP   4.815240   1.325642    0.001964
```

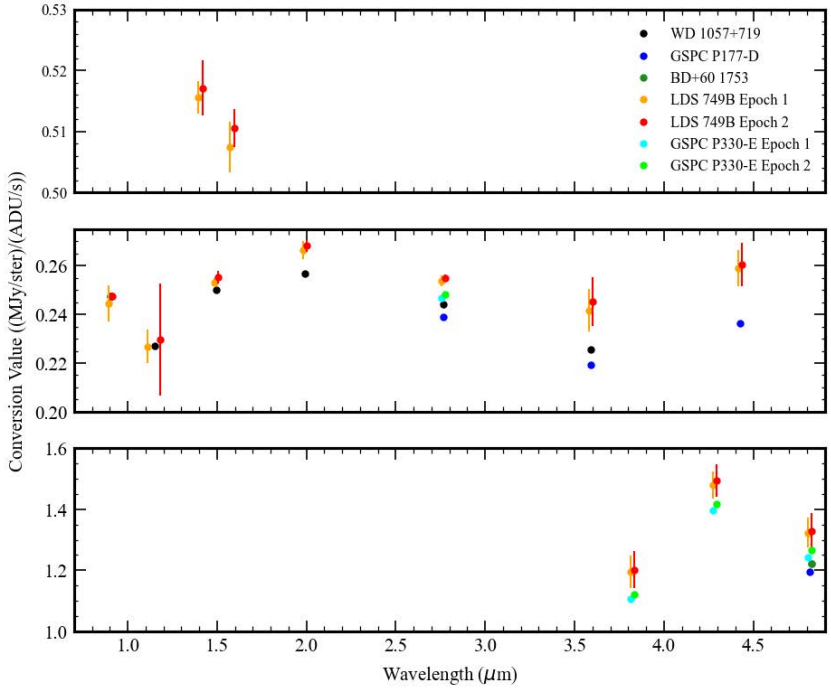

Figure 15: The mean photometric values, with uncertainties, for all the standard stars which have been observed by NIRISS during commissioning.

6.0 Comparison of Different Standard Stars

A number of differences are seen from one standard star to another. The two G-type stars, GSPC P177-D and GSPC P330-E, show lower values than for the hot star measurements taken at the same epoch. The later epoch photometry values are higher than the early photometric observations for both these two stars and between WD 1057+719 and LDS 749B, except for the two shortest wavelength filters F090W and F115W where the values are consistent within the uncertainties. For the early photometric observations, the WD 1057+719 values are about 2% higher than the GSPC P177-D values, and for the NIS-020 observations the LDS749B values for the F277W filter are about 3% higher than the GSPC P330-E values; comparisons in the other long wavelength filters are difficult because of the higher uncertainties in the mean values. Finally, the BD+60°1753 observation in the F480M filter is about 1% higher than the measurement from GSPC P177-D. The value from BD+60°1753 is about 4% lower than the value derived from LDS 749B and about 2% lower than the value from GSPC P330-E, although the nominal uncertainty in the BD+60°1753 observation is much better than those in the NIS 020 observations.

These various small discrepancies are within the general expectation of the standard stars being calibrated to about 2% accuracy at these wavelengths, but they may be pointing to

small systematic differences between the stellar atmosphere models for the hot stars and for the G-type stars. For the initial photometric calibration, the means of the values for LDS 749B from both epochs were used rather than attempting to understand these possible differences with spectral type.

In the NRM case the photometric calibration values used were simply scaled from the normal imaging ones by the expected factor of 0.84/0.15, this being the ratio of the CLEARP to NRM estimated throughputs which are assumed to be uniform with wavelength. This value was verified on orbit to a good accuracy using observations of the background signal in full-frame images in one of the other commissioning programs. Given the uncertainties seen in the individual measurements with the NRM in NIS-020 this was thought to be the more accurate way of estimating the photometric calibration.

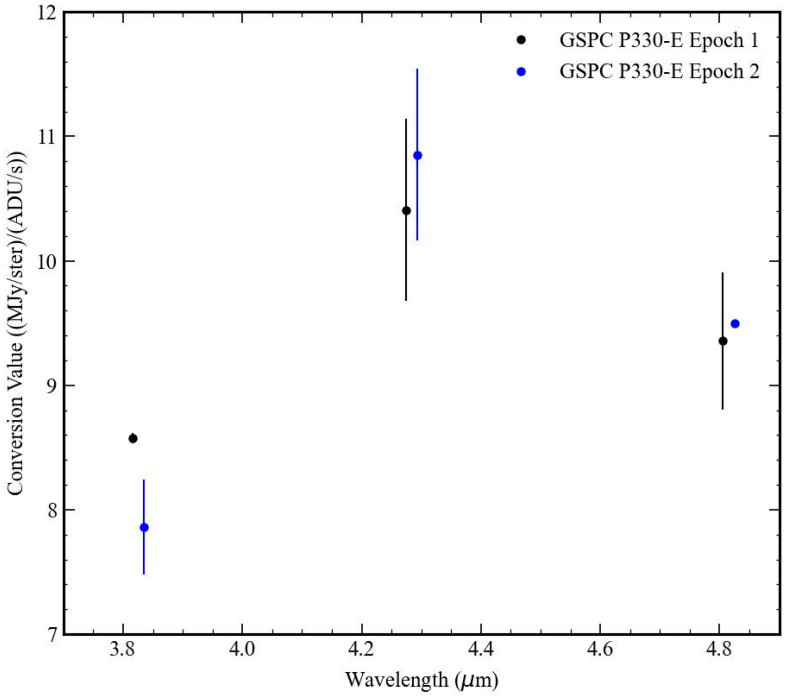

Figure 16: Comparison of the NRM photometric values for the two epochs in the medium-band filters with standard GSPC P330-E. In most cases the precision of the measurements is worse than expected. The F380M value from epoch 1 and the F480M value from epoch 2 have much smaller uncertainties than the other measurements.

7.0 Comparison of the Two Epochs

It is clear from the results shown above that the average epoch 2 photometric values for both LDS 749B and GSPC P330-E are slightly higher than the epoch 1 values. The epoch 2 over epoch 1 ratio varies from 1.003 to 1.015. The values are given in the table below. Averaging the ratio values from all 12 filters gives a mean value of 1.0077, a standard deviation of 0.0036, and a standard deviation in the mean of 0.0011 so the

deviation from 1.0 appears to be statistically significant. It may be that this change is due to variations in the primary mirror properties in the roughly 2 weeks between the observations. There was a fairly significant tilt event in the mirror segments between the two observations, and while this was corrected it may have caused sufficient change to make the difference that is observed between the epochs. The aperture corrections were made from the WebbPSF models but these use the pre-flight optical path difference file rather than being able to use on-orbit measurements. Although the aperture corrections increase with wavelength from about 1.05 for F090W to 1.18 for F480M the ratio values show no trend with wavelength. The significant under-sampling of the NIRISS PSF may mean that the shorter wavelength filters are relatively more vulnerable to optical path difference changes and that this partially compensates for the smaller aperture corrections so that the magnitude of the variations does not rise as the wavelength increases.

Filter	Scaling	Uncertainty	Scaling	Uncertainty	Ratio
	Epoch 1		Epoch 2		
F090W	0.244580	0.007391	0.247343	0.001755	1.01130
F115W	0.226848	0.006747	0.229585	0.023070	1.01207
F140M	0.515652	0.002660	0.517139	0.004569	1.00288
F150W	0.253114	0.001624	0.255267	0.002516	1.00851
F158M	0.507419	0.004190	0.510594	0.003133	1.00626
F200W	0.266312	0.003809	0.268011	0.002491	1.00638
F277W	0.253724	0.002122	0.254875	0.001474	1.00454
F356W	0.241680	0.008592	0.245218	0.009833	1.01464
F380M	1.194465	0.053113	1.202303	0.059696	1.00656
F430M	1.479465	0.044524	1.494832	0.053747	1.01039
F444W	0.258988	0.007352	0.260533	0.008840	1.00597
F480M	1.323678	0.048951	1.327606	0.059633	1.00297

It seems less likely that the NIRISS throughput could change by 1% over such a short time scale, but additional observations in cycle 1 will be needed to rule out such a possibility. Since the two standard stars both show a similar change, it is assumed that this is not due to variations in the stellar brightness between the two observations.

8.0 Persistence Measurements

The two-point dithering of the stars in the observations allows some attempt to measure persistence by looking at the signal at the first stellar position in the dithered image. However, the dither offset is relatively small, about 4.5 pixels in both x and y. This is not far enough to move the possible persistence signal entirely off of the stellar PSF so the result is somewhat of an upper limit value. The automatic code carried out a measurement of the persistence in each pair of images for the NIS 020 observations for LDS 749B, comparing the signal in the 3×3 box on the previous source position in rate image for the second dither position with the signal in the same box on the rate image of the first dither position. The result was a fractional persistence estimate of 0.36%±0.14%. A better measurement would be obtained by doing the same calculation on the PSF model images and taking the difference in the ratio of the real observation and

that from the PSF model, since the theoretical PSF image will have no persistence. That improvement may be added to the code in the future.

9.0 Comparison With Predictions

In principle the imaging conversion values can be simulated from the NIRISS throughput and detector response values along with a few constants such as the estimated OTE primary mirror area. Since the value that is being measured relates the count rate to the photon weighted mean flux density, the conversion value is a weighted average over the NIRISS filter response as well. As there is no specific wavelength information in the photometric conversion values for each filter, the best one can get from the simulations is an estimate of a possible overall scaling of the filter response. The limiting factor for this type of calculation are the uncertainties in the specification of the spectral energy distribution of the standard star in physical units. As discussed above, the variations in the photometric values from the different standard stars may indicate that the models have systematic problems at the 1% level.

Nonetheless a simulation has been carried out for the case of LDS 749B to compare the simulated count rate from the best available CALSPEC stellar model lds749b_mod_007.fits with the observed count rates. Table 3 gives the results for the revised NIRISS throughputs after adjustments to the various NIRISS component throughput files to match the response functions in all the NIRISS observing modes. The adjustments made to the JWST Exposure Time Calculator (ETC) input files are described in a separate technical report (Volk et al., 2022).

The short wavelength filter simulated signal values are close to the measured values. The mean of the ratios of the 6 filters is almost exactly 1.0, and all of the ratio values are consistent with 1 within the measurement uncertainties. The long wavelength filters have ratio values of 1.02 for F444W and F277W, while the ratios for the remaining four filters are slightly less than 1. The ratio values for the long wavelength filters were originally in the range from 1 to 1.1 and an adjustment was made to the long wavelength estimated quantum efficiency to make the agreement better, as discussed in Volk et al. (2022).

Table 3: Results of a simulation of the imaging count rates for LDS 749B with the measured count rates for one observation per filter.

Filter	Count Rate (ADU/s)	Simulated Count Rate	Ratio Observed/Simulated
F090W	113626±2756	113585.5	1.000±0.024
F115W	84632±1847	83622.32	1.012±0.022
F140M	27074±156	26927.47	1.005±0.006

F150W	50101±393	50127.98	0.999±0.008
F158M	22617±143	22909.64	0.987±0.006
F200W	28766±307	28868.17	0.996±0.011
F277W	16845±112	16470.88	1.022±0.007
F356W	10584±464	10641.34	0.995±0.047
F380M	1921±80	1923.68	0.999±0.044
F430M	1236±33	1258.49	0.982±0.029
F444W	6697±216	6549.94	1.022±0.036
F480M	1117±36	1118.25	0.999±0.032

10.0 Variation of Response with Wavelength

One simple diagnostic of the photometric calibration values is to compare these as a function of wavelength, but with a correction for the effect of the different filter widths. One way to make such a correction is to divide the observed signal value by the filter full-width at half maximum (FWHM) using the total combined response function. This is equivalent to multiplying the photometric conversion values by the FWHM value. Figure 17 shows this plot for the average LDS 749B photometry values that were used for the CRDS reference file. The overall trend is smooth although there is some variation between the values for F430M, F444W, and F480M. It is not clear whether the F444W value is low or whether the F430M and F480M values are high compared to the trend from shorter wavelengths. The filter profiles for the F380M, F430M, and F480M filters are much less "box-shaped" and more "triangle-shaped" than is typically the case for the other NIRISS filters. This may skew the FWHM value somewhat in terms of describing the filter width for these filters compared to the others. The run of values in Figure 17 is somewhat different than the pre-launch prediction from simulations and it shows less curvature than was expected. Even so, an order 3 polynomial fit is a fairly good approximation to the data points.

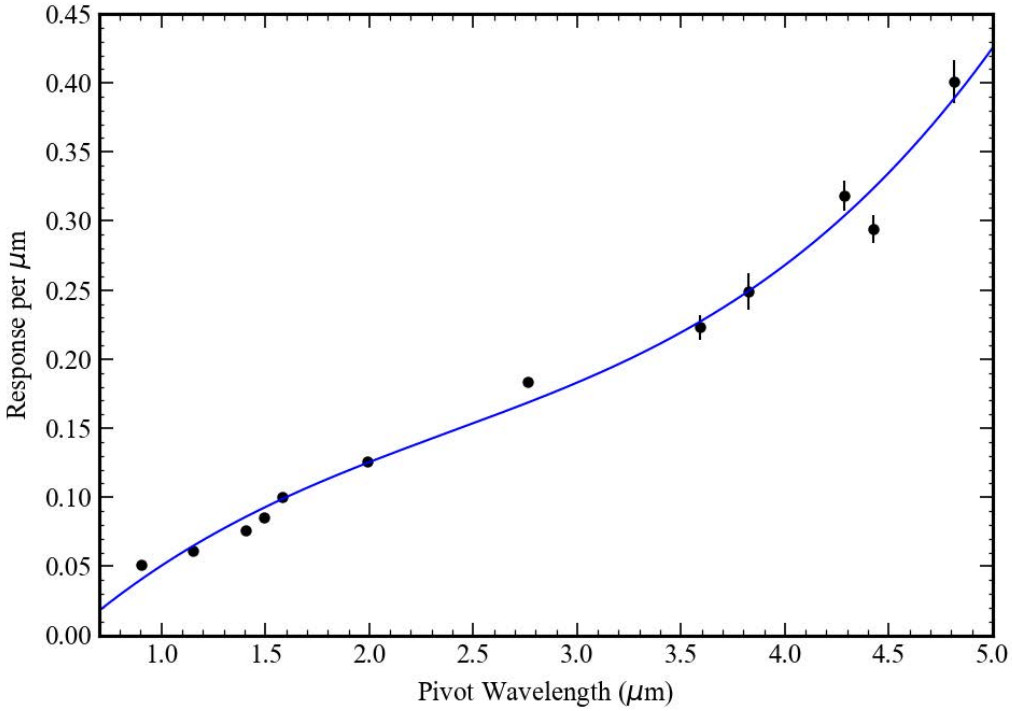

Figure 17: The photometric response in (MJy/ster)/(ADU/s) per micron of filter width, as a function of the pivot wavelength for the NIRISS imaging filters. Also shown is an order 3 Legendre polynomial fit to the data points.

11.0 Conversion to Magnitudes

Although the main goal of the NIS-020 program was limited to providing the conversion values from ADU/s to MJy/ster, the JWST pipeline provides magnitude values in the source catalogue step in level 3 which requires a definition of a magnitude system for NIRISS imaging. The pipeline produces the source catalogue values from resampled images on a fixed pixel scale, and uses this pixel scale to convert back from MJy/ster units to Jansky units. The (aperture corrected) flux density values in Jansky are expressed at AB magnitudes using the zero-magnitude flux density of 3631 Jansky for all filters. To produce the commonly used magnitudes wherein a mean A0V star has colours of 0.0 between the filters the pipeline uses an offset value from AB to "Vega" magnitudes that is provided by the instrument team.

The calculation of these offset values requires using equation (1) to calculate the photon weighted mean flux density values for a star that is assigned a set A0V type magnitude. The values in Jansky are then scaled to zero magnitude and compared the AB zero point of 3631 Jansky to calculate the magnitude offset between the two systems.

Related to this, it is customary to provide a magnitude offset from a count rate of 1 ADU/s to the standard A0V-type magnitudes or to AB magnitudes in imaging data. For

JWST the magnitude system used assumes a template spectrum for Sirius as a "reference" A0V spectral shape, and Sirius is assigned a magnitude of –1.395 in all filters. The Calspec file sirius_mod_004.fits was used as the template spectrum for the calculation. The assigned magnitude for Sirius in the infrared is discussed in Rieke et al. (2022). In the NIRISS case the values are entirely derived from simulations because Sirius is much too bright to observe with JWST. At some later date it may be possible to base these values on a star or stars that NIRISS can observe rather than on a pure simulation. The values are listed in Table 4.

Note that the AB to A0V-type magnitude offset values listed in the Table are defined as a value to subtract from the AB magnitude to get the A0V-type magnitude, which is the convention in the pipeline reference file. For example, a star with an AB magnitude value of 15.00 in the F480M filter has an A0V-type magnitude of 11.5728.

The values in the Table are calculated using the revised total photon conversion efficiency values for NIRISS that were estimated from all the combined photometric measurements in the imaging and spectroscopic modes (see Volk et al. 2022). The on-orbit throughput values are significantly higher than the values that were estimated before launch, typically being 25% higher at most wavelengths. The change in the estimated NIRISS total photon conversion efficiency values is mostly due to a higher estimate for the detector quantum efficiency compared to the pre-launch estimate. There is no indication that the filter response profiles by themselves have changed from the original measurements made when the filters were produced.

Table 4: Zero-Magnitude Values For The NIRISS Imaging Filters

Filter	Zero Magnitude Count Rate (ADU/s)	Magnitude for 1 ADU/s	Zero Magnitude Mean Flux Density (Jansky)	AB to A0V Magnitude Offset
F090W	9.3736e+10	27.4298	2318.88	0.4869
F115W	7.7172e+10	27.2187	1795.54	0.7646
F140M	2.5322e+10	26.0087	1316.64	1.1014
F150W	4.7322e+10	26.6876	1205.08	1.1975
F158M	2.1696e+10	25.8381	1091.72	1.3048
F200W	2.8592e+10	26.1406	766.46	1.6888
F277W	1.6718e+10	25.5580	432.68	2.3097
F356W	1.1033e+10	25.1068	271.32	2.8164
F380M	1.9864e+09	23.2452	237.24	2.9621
F430M	1.3140e+09	22.7965	191.58	3.1942
F444W	6.8348e+09	24.5868	182.99	3.2440

F480M	1.1706e+09	22.6710	154.58	3.4272

12.0 Conclusions

The data reduction and analysis of the NIRISS imaging photometry measurements taken during JWST commissioning has been presented. There are some indications of a variation from one photometric standard star to another at the 1% to 2% level, and also some indication of a smaller level of variation with time which is tentatively attributed to changes in the OTE optical path differences rather than to changes in the NIRISS instrument. Both of these things will need to be tested with further observations in future calibration observations during regular JWST operations.

13.0 References

Bohlin, R. C., Gordon, K. D., and Tremblay, P.-E., 2014, PASP, 126, 711.

Goudfrooij, P., et al., 2022, "NIRISS Commissioning Results: NIS-020 – NIRISS Photometric Zeropoints (NGAS CAR-707, APT 1094)", JWST Technical Report JWST-STScI-008267.

Perrin, M., D., Sivaramakrishnan, A., LaJoie, C.-P., Eloit, E., Pueyo, L., Ranvindranath, S., and Alvert, L., 2014, Proc. SPIE. 9143.

Rieke, G. H., Su, K., Sloan, G. C., and Schlawin, E., 2022, AJ, 163, 45.

Volk, K., et al., 2022, "NIRISS Throughput Calibration", JWST Technical Report JWST-STScI-008268, SM-12.